Supporting information

Discovery and optimization of the first ATP competitive Type-III c-MET inhibitor

Iacovos N. Michaelides,*[†] Gavin W. Collie,[†] Ulf Börjesson,[‡] Christina Vasalou,[⁘] Omar Alkhatib,[†] Louise Barlind,[‡] Tony Cheung,[⁙] Ian L. Dale,[†] Kevin J. Embrey,[†] Edward J. Hennessy,[⁜] Puneet Khurana,[†] Cheryl M. Koh,[⁙] Michelle L. Lamb,[⌂] Jianming Liu,[‡] Thomas A. Moss,[◊] Daniel J. O'Neill,[†] Christopher Phillips,[†] Joseph Shaw,[†] Arjan Snijder,[‡] R. Ian Storer,[†] Christopher J. Stubbs,[†] Fujin Han,[┼] Chengzhi Li,[┼] Jingchuan Qiao,[┼] Dong-Qing Sun,[┼] Jingwen Wang,[┼] Peng Wang,[┼] Wenzhen Yang[┼]

[†] Discovery Sciences, R&D, AstraZeneca, Cambridge, CB4 0WG, UK
[‡] Discovery Sciences, R&D, AstraZeneca, 43183 Mölndal, Sweden
[⁘] DMPK, Oncology R&D, AstraZeneca, Boston, Waltham, Massachusetts 02451, US
[⁙] Bioscience, Oncology R&D, AstraZeneca, Boston, Waltham, Massachusetts 02451, US
[⁜] Medicinal chemistry, Oncology R&D, AstraZeneca, Boston, Waltham, Massachusetts 02451, US
[⌂] Computational chemistry, Oncology R&D, AstraZeneca, Boston, Waltham, Massachusetts 02451, US
[◊] Medicinal chemistry, Oncology R&D, AstraZeneca, Cambridge, CB4 0WG, UK
[┼] Pharmaron Beijing Co., Ltd., 6 Taihe Road BDA, 100176 Beijing, People's Republic of China

Corresponding author: Iacovos N. Michaelides − Discovery Sciences, R&D, AstraZeneca, Cambridge, CB4 0WG, UK; https://orcid.org/0000-0001-6993-6788 ; Email: iacovos.michaelides@astrazeneca.com

Table of contents

NMR experiments:

NMR screening:

A detailed description of the NMR screen, using the isolated kinase domain of WT c-MET, has been previously described.[1]

Bespoke NMR experiments:

Compound observed NMR experiments (Carr-Purcell-Meiboom-Gill sequence (CPMG) and WaterLOGSY[2] experiments were performed to monitor binding effects of both adenosine and **2** to human WT or D1228V His6-cMet(1038-1348) c-MET protein. To a sample containing adenosine (500 μM) successive additions of WT c-MET protein (7.4 μM) and **2** (100 μM) clearly illustrated that **2** binding attenuates the binding effect observed for adenosine. The samples were prepared in 5 mm NMR tubes in 25 mM HEPES pH 7.5, 50 mM NaCl, 2 mM $MgCl_2$, 0.02% NaN_3, 5% D_2O. These experiments were performed on a Bruker Avance III 600 MHz spectrometer with a triple resonance inverse cryoprobe equipped with z-axis gradients.

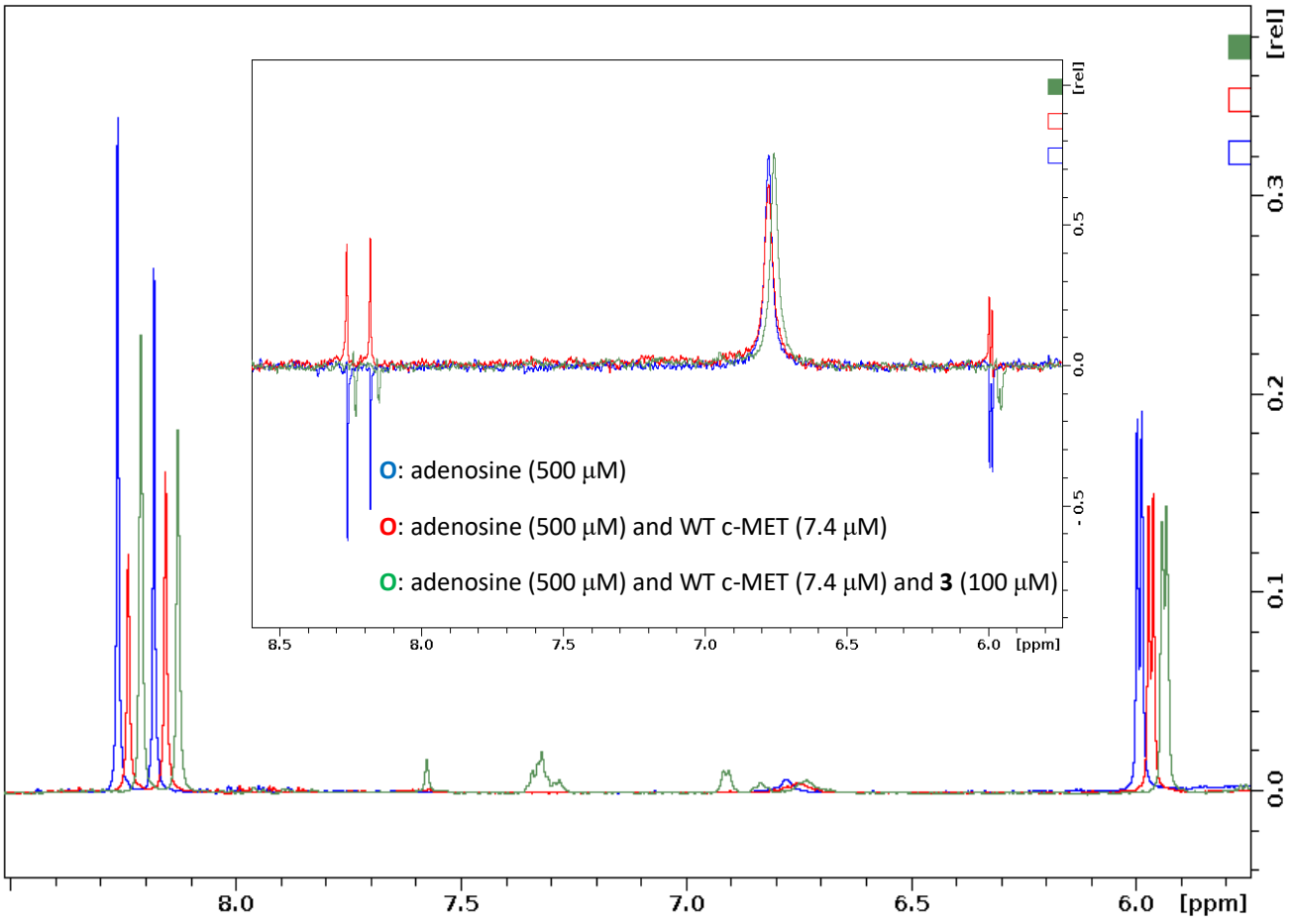

Figure S1. NMR studies of fragment hit **2**.

Regions of CPMG spectra under identical conditions, with WaterLOGSY spectra of the samples shown in the insert, containing adenosine (500 μM) in blue, after the addition of WT c-MET (7.4 μM) in red and after the further addition of **2** (100 μM) in green. In the CPMG experiments, the addition of WT c-MET results in significant decrease of the adenosine resonances, indicative of adenosine binding to the

protein. Following the addition of **2** to a pre-equilibrated sample of adenosine and WT c-MET there is partial recovery of the H2 and H8 adenine resonances which is indicative of **2** having competitive binding with adenosine. Equivalent changes occur in the WaterLOGSY spectra and the results are consistent with the CPMG data.

Crystallography

Experimental details

For crystallization trials, purified recombinant protein samples encompassing residues 1038-1346 of wild-type or D1228V c-MET were used at a concentration of around 10 mg/ml. A detailed description of the protein expression and purification methods has been reported previously.[1, 3, 4] All inhibitor complex crystal structures reported in this work were obtained by co-crystallization. Inhibitors were added to c-MET to a final concentration of 1 mM from 100 mM stocks in 100% DMSO. All inhibitor complexes were screened against 200-400 sparse matrix conditions in order to find suitable crystallization conditions using the sitting drop method in 96 well plates, with final drop volumes of around 200 *n*L. For data collection, crystals were either frozen directly in liquid nitrogen or cryo-protected before freezing. Diffraction data were collected at the SOLEIL and Diamond Light Source synchrotrons. Diffraction data were processed using DIALS, xia2, XDS, CCP4 and autoPROC.[5-9] Structures were solved by molecular replacement using Phaser[10] using publicly available search models.[4, 11-13] Structures were refined using Buster (Global Phasing Ltd.) with geometric restraints for small molecule ligands generated using Grade (Global Phasing Ltd.) and model building performed in Coot.[14] Further details concerning crystallization, data collection and refinement can be found in **Table S1**. Coordinates and structure factors have been deposited in the Protein Data Bank with accession codes provided in **Table S1**.

Crystal structures

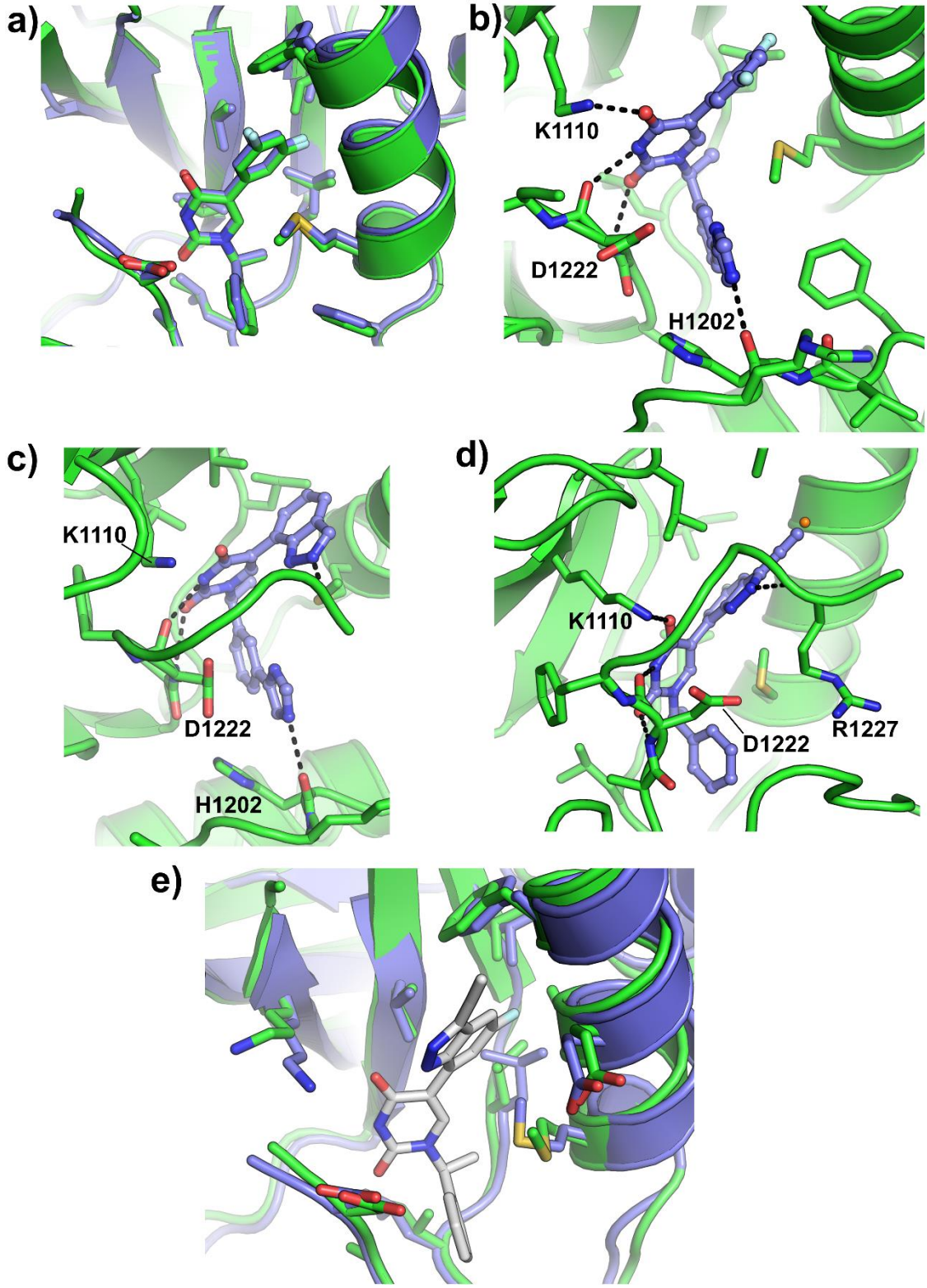

Figure S2. a) Alignment of crystal structures of wild-type (blue carbons) and D1228V (green carbons) c-MET bound by compound **2**. b) Crystal structure of D1228V c-MET in complex with compound **10**. c) Crystal structure of D1228V c-MET bound by compound **16**. d) Crystal structure of D1228V c-MET bound by compound **29**. Water **III** from the c-MET-**15** complex is shown as an orange sphere. e) Alignment of the back-pockets of c-MET (white and blue carbons, PDB entry 8OUU) and MER (green carbons, PDB entry 7AAX[15]).

Table S1. X-ray data collection and refinement statistics for c-MET crystal structures.

c-MET form	Wild-type	D1228V	D1228V
Compound	**2**	**2**	**10**
Crystallization conditions	12% PEG3350, 5% EtOH, 0.2 M Li_2SO_4, 0.1 M PCTP* pH 5	15% PEG2000 MME, 0.1 M PCTP* pH 6.5	1.5 M LiCl, 0.1 M Na HEPES pH 7.5
Data Collection			
Space group	C2	$P2_12_12$	$P4_12_12$
Unit cell			
a, b, c (Å)	123.66, 45.61, 53.76	254.82, 46.20, 81.06	111.64, 111.64, 130.43
α, β, γ (°)	90.00, 108.29, 90.00	90.00, 90.00, 90.00	90.00, 90.00, 90.00
Resolution (Å)	46.40 – 2.27 (2.33 – 2.27)	254.82 – 2.63 (2.68 – 2.63)	78.98 – 1.95 (1.98 – 1.95)
R_{meas} (%)	13.2 (87.1)	22.5 (162.0)	15.5 (234.7)
$CC_{1/2}$ (%)	99.4 (73.9)	99.3 (54.2)	99.8 (51.2)
I / σ	6.4 (1.6)	6.7 (1.3)	9.6 (1.3)
Completeness (%)	98.8 (92.6)	100 (99.7)	100 (99.8)
Reflections (total)	44554	188848	760675
Reflections (unique)	13200	29537	60639
Redundancy	3.4	6.4	9.6
Refinement			
Resolution (Å)	46.40 – 2.27	81.06 – 2.63	28.27 – 1.95
R / R_{free} (%)	24.5 / 29.5	28.06 / 32.92	27.3 / 28.7
Overall B-factor (Å^2)	47.66	41.58	33.82
R.m.s. deviations			
Bond lengths (Å)	0.008	0.007	0.008
Bond angles (°)	0.89	0.84	0.90
PDB code	8OW3	8OWG	8OV7

*PCTP = Sodium propionate, sodium cacodylate trihydrate, bis-tris propane.

Table S1 continued.

c-MET form	D1228V	D1228V	D1228V
Compound	**15**	**16**	**29**
Crystallization conditions	30% PEG400, 0.1 M $CaCl_2$, 0.1 M PCTP* pH 4.5	12% PEG 8000, 200 mM NH_4I, 0.1 M PCTP* pH 7	2 M Na formate, 0.1 M Na acetate pH 4.6
Data Collection			
Space group	$P2_12_12_1$	$P2_12_12_1$	$P2_12_12_1$
Unit cell			
a, b, c (Å)	53.77, 56.23, 215.95	53.90, 56.67, 215.81	53.63, 56.74, 214.77
α, β, γ (°)	90.00, 90.00, 90.00	90.00, 90.00, 90.00	90.00, 90.00, 90.00
Resolution (Å)	215.95 – 1.78 (1.81 – 1.78)	44.52 – 2.21 (2.26 – 2.21)	71.59 – 1.77 (1.80 – 1.77)
R_{meas} (%)	6.4 (48.3)	14.6 (98.3)	10.2 (111.5)
$CC_{1/2}$ (%)	99.9 (91.4)	99.2 (65.3)	99.8 (72.9)
I / σ	16.1 (2.2)	7.4 (1.6)	9.5 (1.4)
Completeness (%)	98.6 (86.2)	98.8 (95.0)	99.9 (97.8)
Reflections (total)	381926	163653	398434
Reflections (unique)	62697	33771	64902
Redundancy	6.1	4.8	6.1
Refinement			
Resolution (Å)	107.97 – 1.78	39.08 – 2.21	54.86 – 1.77
R / R_{free} (%)	19.12 / 21.97	22.5 / 27.5	20.21 / 22.51
Overall B-factor (Å^2)	29.69	41.47	33.47
R.m.s. deviations			
Bond lengths (Å)	0.009	0.007	0.009
Bond angles (°)	0.91	0.87	0.91
PDB code	8OUV	8OVZ	8OUU

*PCTP = Sodium propionate, sodium cacodylate trihydrate, bis-tris propane.

DMPK experiments:

Materials

Human liver microsomes (150 donors; Lot QQY and Lot 38289) were purchased from Corning or BioIVT (Shanghai, China), respectively. Human hepatocytes (10 donors; Lot LYB and Lot IRK) were purchased from BioIVT. Male Han Wistar Rat hepatocytes and rat plasma were obtained from BioreclamationIVT. The Rapid Equilibrium Device (RED) were purchased from Gibco by Thermo Fisher Scientific (Shanghai, China). Male Wistar Han rats were purchased from Vital River. The experimental work for all *in vitro* and *in vivo* assays described below was conducted at the Contract Research Organization, Pharmaron, China.

Methods

Well established methods for hepatocyte and liver microsome intrinsic clearance, Clint, permeability, cell efflux ratio and protein binding utilized throughout this work have been described in detail elsewhere.[16] A general overview of these methods is provided below. Specifics around assay conditions and data analysis for the remaining assays of brain protein binding, *in vivo* plasma PK and brain penetration profiling in rat are noted in the text below.

Rat and human hepatocyte Clint

The hepatocyte incubations were prepared in Leibovitz's L-15 Medium pH 7.4 containing 1 million hepatocytes/mL and a final compound concentration of 1 μM. Cell viability was determined using a Cellometer Vision and >80% cell viability was required to proceed with the compound incubation. The compound/cell solution (250 μL) was incubated for 2 hours at 37 ^{o}C and shaken at 900 rpm on an Eppendorf Thermomixer Comfort plate shaker. Samples (20 μL) were taken at 0.5, 5, 15, 30, 45, 60, 80, 100 and 120 min and quenched with 100 μL of 100% ice cold acetonitrile. Samples were analyzed by LC-MS/MS.

Human liver microsome Clint

The microsomal incubations were prepared in phosphate buffered solution pH 7.4 containing 1 mg/mL microsomal protein, 1 mM NADPH and a final compound concentration of 1 μM. Following a pre-incubation with NADPH for 8 min, reactions were initiated through the addition of the test compound (final volume 250 μL) and incubated at 37 °C in a water bath for 30 min. At each timepoint (0.5, 5, 10, 15, 20, 30 min) 20 μL of incubation mixture was quenched with 100 μL of 100% ice cold acetonitrile. Samples were analyzed by LC-MS/MS.

Determination of CaCo-2 or MDCK-MDR1 permeability and cell efflux ratio

CaCo-2 cells were plated at $6.86x10^5$ cells/mL and were cultured at 14-18 days with culture medium replaced every other day. MDCK-MDR1 cells were plated at $1.56x10^6$ cells/mL and were cultured for 4-8 days with culture medium replaced every other day. Experiments were performed by adding 10 μM of the test compound in the donor well and measuring the appearance in the receiver well after 2 hours incubation at 37 ^{o}C. The donor well is the apical (A) compartment and the receiver is the basolateral (B) compartment, when determining the rate of compound transport in the apical to basolateral (A-B) direction. Similarly, the donor well is the basolateral (B) compartment and the receiver is the apical (A) compartment, when determining the rate of compound transport in the basolateral to apical (B-A) direction. Samples were analyzed by LC-MS/MS.

Plasma protein binding in rat

Plasma protein binding was completed using a RED device. Experiments were performed by adding 5 μM of test compound to the donor chamber and phosphate buffered solution pH 7.4 to the receiver

chamber. The plate was incubated for 18 hours at 37 ^{o}C. Compound recovery and stability in plasma was determined using samples at time T=0 and T=18 h. Samples were analyzed by LC-MS/MS.

Brain protein binding in rat

The *in vitro* free fraction of compound in rat brain was measured *via* a brain slice assay as described by Fridén *et al*.[17] Freshly prepared slices from rat brain were incubated in ECF buffer solution at pH 7.4 spiked with a cassette of compounds for 5 hours at 37^{o} C. The final concentration of each test compound was 0.1 μM and the total concentration in the cassette did not exceed 1 μM. The concentrations were measured for the slice and buffer by LC/MS/MS. The unbound volume of distribution and the free fraction of the test compound was computed as indicated in equations 1 and 2.

In vivo plasma and brain exposure in rat

The plasma pharmacokinetic profile of test compounds was determined *via* intravenous (IV) and oral administration (PO) in male Han Wistar rats. The dose level was set at 0.5 mg/kg (dose volume of 1 mL/kg) for intravenous administration, dosed to 2 animals, and 1 mg/kg (dose volume of 4 mL/kg) for oral administration, dosed to 2 animals. Test compounds were administered as a cassette up to 5 test compounds, either intravenously *via* tail vein for IV dosing or *via* oral gavage for PO dosing. Plasma samples were collected *via* the jugular vein at prespecified time points: pre-dose, 2, 5, 10, 30 min, 1, 2, 4, 8, 24 hours post dose for IV administration and pre-dose, 15, 30 min, 1, 1.5, 2, 3, 4, 8, 24 hours post dose for PO administration. All samples were analyzed by LC-MS/MS. Pharmacokinetic parameters – such as clearance (CL), volume of distribution (V_{ss}) and bioavailability – were computed *via* noncompartmental analysis using appropriate software such as WinNonlin Phoenix.

The brain to plasma exposure of test compounds was determined in three male Han Wistar rats following intravenous infusion administration for 4 hours as described by Fridén *et al.*[18] All animals had free access to food and water. Compounds were administered as a cassette up to 3 test compounds. The dose level of each test compound was set at 2 μmol/kg/h. Rats were dosed *via* the jugular vein using a venous catheter and blood was collected by heart puncture. Brain and plasma samples were collected at the terminal time point of infusion, i.e. 4 hours, and analyzed by LC-MS/MS.

Rats assigned to the study were sourced from Beijing Vital River Laboratory Animal Technology Co., Ltd, China. Animals were housed in Polycarbonate animal cage (3 animals per cage during the acclimation and single animal per cage after jugular vein surgery). Absorbent corncob bedding was used for the collection and absorption of excreta from animals. Animals were free access to food with Rodent Diet from Beijing Keaoxieli, irradiated by Cobalt-60. The sterile water was provided *ad libitum* via water containers. Animals were housed in a controlled environment (set up to maintain 20-25 °C and 40-70% relative humidity). A 12-hour light/12-hour dark cycle was maintained except when interrupted by study-related events. An animal care and use application for this study was submitted to Pharmaron's Institutional Animal Care and Use Committee (IACUC) for approval in accordance with Pharmaron's IACUC policies and procedures.

Data analysis

The free fraction in rat brain $f_{u,brain}$ was calculated according to the following equations:

$$V_{u,brain} = \frac{C_{slice} - V_o * C_{ECF}}{(1 - V_o) * C_{ECF}} \quad (1)$$

$$f_{u,brain} = \frac{1}{V_{u,brain}} \quad (2)$$

Where C_{slice} is the amount of drug in the brain slice, C_{ECF} is the drug concentration in extracellular fluid buffer (ECF) and V_o the water adhesion of the brain slice. V_0 is 0.0931, i.e. on average 9.31% water is assumed to adhere to the brain slices.

The brain to plasma concentration ratio, K_p, was determined based on the following equation:

$$K_p = \frac{C_{brain}}{C_{plasma}} = \frac{C_{homogenate} - 0.008 * C_{plasma}}{C_{plasma}} \quad (3)$$

The brain concentration (C_{brain}) was corrected for residual blood by subtracting 0.8% of the plasma concentration (C_{plasma}) from the total brain homogenate, i.e. $C_{homogenate}$.

The unbound brain ($C_{brain,u}$) to plasma ($C_{plasma,u}$) concentration ratio, $K_{p,uu}$, has been computed as follows:

$$K_{p,uu} = \frac{C_{brain,u}}{C_{plasma,u}} = K_p \frac{fu_{brain}}{fu_{plasma}} \quad (4)$$

Where $f_{u,brain}$ and $f_{u,plasma}$ are the free fractions of test compound in brain and plasma respectively.

Kinase selectivity data

Compounds **30** and **32** were screened at a concentration of 100 nM against a panel of 140 kinases using ThermoFisher's SelectScreen Kinase Profiling Service. Compound **31** was screened at a concentration of 1 μM against a panel of 144 kinases (additional kinases: MET D1228H, MERTK (cMER) A708S, AXL R499C, FLT3 ITD). Further details provided in **Table S2**, **Table S3** and **Table S4**.

Table S2. Kinase selectivity data for **30** at 100 nM

Kinase Name	Mean Inhibition (%)
MERTK (cMER)	100.7
MET (cMet)	86.4
TYRO3 (RSE)	47.7
AXL	41.4
MST1R (RON)	38.6
RPS6KB1 (p70S6K)	18.6
CAMK1 (CaMK1)	14.4
IRAK4	11.7
PIK3C2A (PI3K-C2 alpha)	11.7
MAPKAPK2	11.6
NTRK3 (TRKC)	11.4
MAP3K9 (MLK1)	11.0
LCK	10.5
PRKCQ (PKC theta)	10.2
PRKCA (PKC alpha)	9.6
PTK6 (Brk)	9.4
SRC	8.4
DYRK2	7.9
IGF1R	7.8
INSR	7.7
ALK	7.7
FES (FPS)	7.4
PIK3CG (p110 gamma)	7.4
PRKCE (PKC epsilon)	7.2
INSRR (IRR)	6.9
FRAP1 (mTOR)	6.8
CSNK1G1 (CK1 gamma 1)	6.6
MAP2K1 (MEK1)	6.6
CAMK2B (CaMKII beta)	6.5
PEAK1	6.5
CDK2/cyclin A	6.3
RPS6KA1 (RSK1)	6.2
NTRK2 (TRKB)	6.2
CDK1/cyclin B	5.9
PAK1	5.7
EPHA5	5.4
KDR (VEGFR2)	5.3
PRKG1	5.1
NTRK1 (TRKA)	5.0
CSF1R (FMS)	4.9
FLT3	4.9
ROS1	4.7
PAK7 (KIAA1264)	4.5
RAF1 (cRAF) Y340D Y341D	4.4
TBK1	4.4
MARK1 (MARK)	4.1
PDK1	4.0
AKT2 (PKB beta)	4.0
CLK1	3.9
LRRK2	3.8
PTK2 (FAK)	3.8
CLK2	3.8
RET V804L	3.6
ROCK1	3.5
TGFBR1 (ALK5)	3.4
BTK	3.4
PIK3C3 (hVPS34)	3.3
CDK7/cyclin H/MNAT1	3.3
RET	3.2
PIM2	3.2
PDGFRB (PDGFR beta)	3.1
SRPK1	3.1
ROCK2	3.0
FGFR1	2.9
PLK1	2.9
MAP4K1 (HPK1)	2.7
ABL2 (Arg)	2.4
EEF2K	2.3
RET V804M	2.3
MAPK14 (p38 alpha) Direct	2.1
ZAP70	2.0
MARK2	2.0
MINK1	2.0
FLT1 (VEGFR1)	1.9
EPHB1	1.9
MAPKAPK5 (PRAK)	1.8
PAK2 (PAK65)	1.7
FGFR2	1.6
SYK	1.6
MAPK8 (JNK1)	1.5
FER	1.5
CSNK2A2 (CK2 alpha 2)	1.5
AKT1 (PKB alpha)	1.4
EPHB4	1.4
STK17A (DRAK1)	1.1
EGFR (ErbB1)	0.9
AMPK A2/B1/G1	0.9
FYN	0.7
LYN A	0.7
PAK4	0.6
MAPK1 (ERK2)	0.5
NEK2	0.5
NUAK1 (ARK5)	0.4
AURKB (Aurora B)	0.1
KIT	0.1
PRKACA (PKA)	0.0
FGFR4	0.0
AAK1	-0.1
MYLK (MLCK)	-0.2
TNIK	-0.3
CLK3	-0.8
CLK4	-0.9
PIK3CD/PIK3R1 (p110 delta/p85 alpha)	-0.9
STK4 (MST1)	-0.9
DDR2	-1.1
CHEK1 (CHK1)	-1.2
JAK1	-1.2
AURKC (Aurora C)	-1.2
CDK8/cyclin C	-1.5

DNA-PK	-1.6
CDK9/cyclin T1	-1.8
SGK (SGK1)	-1.8
RPS6KA5 (MSK1)	-1.9
GSK3A (GSK3 alpha)	-1.9
MAP4K3 (GLK)	-1.9
ABL1	-2.2
IKBKB (IKK beta)	-2.2
PI4KB (PI4K beta)	-2.5
FGFR3	-2.7
PIK3CB/PIK3R1 (p110 beta/p85 alpha)	-2.8
BRAF	-2.9
MAP3K7/MAP3K7IP1 (TAK1-TAB1)	-3.0
JAK2	-3.0
ACVR1B (ALK4)	-3.3
ULK2	-3.5
YES1	-3.5
GSK3B (GSK3 beta)	-3.5
DMPK	-4.0
FGFR1 V561M	-4.7
CDK2/cyclin E1	-4.8
EGFR (ErbB1) T790M L858R	-4.9
BLK	-5.4
GSG2 (Haspin)	-5.9
IRAK1	-7.0
BMX	-7.4
MKNK2 (MNK2)	-7.9
ERBB2 (HER2)	-8.5
PIK3CA/PIK3R1 (p110 alpha/p85 alpha)	-10.7
JAK3	-12.1
ERBB4 (HER4)	-16.5

Table S3. Kinase selectivity data for **32** at 100 nM

Kinase Name	Mean Inhibition (%)
MET (cMet)	83.9
MERTK (cMER)	75.3
MST1R (RON)	47.6
TYRO3 (RSE)	30.8
PIK3CB/PIK3R1 (p110 beta/p85 alpha)	16.0
IRAK4	14.7
PRKCQ (PKC theta)	13.6
AXL	13.4
SRC	12.9
NTRK3 (TRKC)	12.1
MAP2K1 (MEK1)	12.0
NEK2	12.0
MAPKAPK2	11.8
IRAK1	11.5
NTRK1 (TRKA)	11.2
PIK3C2A (PI3K-C2 alpha)	10.5
FRAP1 (mTOR)	10.4
RPS6KB1 (p70S6K)	10.2
ALK	10.0
FES (FPS)	10.0
PI4KB (PI4K beta)	9.3
INSR	9.0
EPHA5	8.9
CLK4	8.9
CDK9/cyclin T1	8.9
LCK	8.8
IGF1R	8.7
PIK3C3 (hVPS34)	8.6
MAPK8 (JNK1)	8.2
MAP3K9 (MLK1)	8.0
RPS6KA1 (RSK1)	7.4
CLK2	7.4
FGFR4	7.2
INSRR (IRR)	7.1
CDK7/cyclin H/MNAT1	6.9
LYN A	6.6
KDR (VEGFR2)	6.6
RET	6.5
ROCK1	6.5
CAMK2B (CaMKII beta)	6.4
FLT3	6.2
PAK1	6.0
TBK1	6.0
LRRK2	5.9
ABL2 (Arg)	5.9
CAMK1 (CaMK1)	5.7
MINK1	5.6
PTK6 (Brk)	5.5
EPHB4	5.5
FGFR1	5.4
MARK2	5.2
ROS1	5.1
PRKACA (PKA)	5.1
PEAK1	5.1
PAK7 (KIAA1264)	5.1
MARK1 (MARK)	4.9
AURKB (Aurora B)	4.9
PIK3CD/PIK3R1 (p110 delta/p85 alpha)	4.9
PDK1	4.7
AAK1	4.6
GSG2 (Haspin)	4.5
PTK2 (FAK)	4.5
PIM2	4.5
RET V804L	4.5
CDK1/cyclin B	4.4
PRKCA (PKC alpha)	4.2
EEF2K	4.2
FGFR2	4.2
PAK2 (PAK65)	4.1
CLK1	4.1
PRKCE (PKC epsilon)	4.1
PDGFRB (PDGFR beta)	4.0
AMPK A2/B1/G1	4.0
MAPK14 (p38 alpha) Direct	4.0
AKT2 (PKB beta)	3.8
FER	3.7
NTRK2 (TRKB)	3.7
CDK2/cyclin A	3.6
SYK	3.3
NUAK1 (ARK5)	3.3
SRPK1	3.3
CSNK2A2 (CK2 alpha 2)	3.3
DMPK	3.2
MAPKAPK5 (PRAK)	3.0
PLK1	2.9
FGFR3	2.9
CSNK1G1 (CK1 gamma 1)	2.6
RAF1 (cRAF) Y340D Y341D	2.5
MKNK2 (MNK2)	2.5
MAP3K7/MAP3K7IP1 (TAK1-TAB1)	2.5
EGFR (ErbB1)	2.4
FLT1 (VEGFR1)	2.0
RPS6KA5 (MSK1)	2.0

PIK3CG (p110 gamma)	1.9
EPHB1	1.8
STK4 (MST1)	1.6
BTK	1.6
TGFBR1 (ALK5)	1.5
AURKC (Aurora C)	1.4
MYLK (MLCK)	1.4
FYN	1.4
MAPK1 (ERK2)	1.3
ROCK2	1.2
CSF1R (FMS)	1.1
AKT1 (PKB alpha)	0.9
DDR2	0.9
IKBKB (IKK beta)	0.8
CLK3	0.7
JAK1	0.7
PRKG1	0.5
PAK4	0.2
GSK3B (GSK3 beta)	-0.1
GSK3A (GSK3 alpha)	-0.2
DYRK2	-0.2
TNIK	-0.3
BRAF	-0.3
RET V804M	-0.3
KIT	-0.4
ZAP70	-0.4
STK17A (DRAK1)	-0.6
SGK (SGK1)	-0.7
ERBB2 (HER2)	-0.7
JAK2	-1.0
MAP4K1 (HPK1)	-1.4
BMX	-1.6
CDK8/cyclin C	-1.7
MAP4K3 (GLK)	-2.5
ULK2	-2.7
CHEK1 (CHK1)	-3.2
JAK3	-3.2
DNA-PK	-3.2
ACVR1B (ALK4)	-3.4
YES1	-3.4
ABL1	-3.6
EGFR (ErbB1) T790M L858R	-3.6
FGFR1 V561M	-4.4
BLK	-5.3
PIK3CA/PIK3R1 (p110 alpha/p85 alpha)	-6.2
CDK2/cyclin E1	-9.0
ERBB4 (HER4)	-15.6

Table S4. Kinase selectivity data for **31** at 1 μM

Kinase Name	Mean Inhibition (%)
MET D1228H	100.0
MERTK (cMER)	99.6
MERTK (cMER) A708S	90.4
MET (cMet)	89.8
TYRO3 (RSE)	79.0
AXL R499C	67.6
MST1R (RON)	66.6
AXL	46.0
TGFBR1 (ALK5)	25.2
CDK9/cyclin T1	20.9
GSG2 (Haspin)	18.9
MAP2K1 (MEK1)	17.2
ZAP70	16.2
PRKACA (PKA)	15.6
RAF1 (cRAF) Y340D Y341D	15.5
PIK3CG (p110 gamma)	14.7
MAPKAPK2	13.1
NTRK1 (TRKA)	13.1
DNA-PK	12.8
IRAK4	12.3
NTRK3 (TRKC)	12.3
IRAK1	11.6
FGFR1 V561M	11.4
PDK1	11.3
CLK4	11.2
MARK1 (MARK)	11.2
ALK	11.2
MAP4K1 (HPK1)	11.0
MKNK2 (MNK2)	9.9
PRKCA (PKC alpha)	9.8
PLK1	9.8
SRC	9.4
FGFR3	9.3
MAP4K3 (GLK)	9.1
STK17A (DRAK1)	9.1
MAP3K7/MAP3K7IP1 (TAK1-TAB1)	9.1
PIK3C2A (PI3K-C2 alpha)	8.9
RET V804M	8.9
PRKG1	8.8
RET	8.7
PIK3CD/PIK3R1 (p110 delta/p85 alpha)	8.6
ULK2	8.6
RPS6KA1 (RSK1)	8.5
INSR	8.5
CLK3	8.3
FLT3	8.0
CDK2/cyclin A	7.7
FYN	7.6
RPS6KA5 (MSK1)	7.6
MAPK1 (ERK2)	7.2
CHEK1 (CHK1)	7.0
AMPK A2/B1/G1	6.9
CDK1/cyclin B	6.8
FER	6.8
AURKB (Aurora B)	6.7
SRPK1	6.7
PDGFRB (PDGFR beta)	6.6
TBK1	6.5
CDK8/cyclin C	6.2
LYN A	6.0
CSF1R (FMS)	5.8
MAPKAPK5 (PRAK)	5.8
MARK2	5.8
PTK2 (FAK)	5.6
CSNK2A2 (CK2 alpha 2)	5.4
CSNK1G1 (CK1 gamma 1)	5.4
FES (FPS)	5.3
PTK6 (Brk)	5.2
MAP3K9 (MLK1)	5.0
EPHB1	4.9
RET V804L	4.9
AAK1	4.8
GSK3A (GSK3 alpha)	4.6
EEF2K	4.5
CAMK2B (CaMKII beta)	4.3
ROCK2	4.2
MYLK (MLCK)	4.0

EPHA5	4.0
EPHB4	3.8
PIK3C3 (hVPS34)	3.8
FGFR1	3.8
PRKCE (PKC epsilon)	3.8
ACVR1B (ALK4)	3.8
CLK1	3.7
AKT1 (PKB alpha)	3.7
GSK3B (GSK3 beta)	3.7
STK4 (MST1)	3.7
PAK1	3.4
BLK	3.1
NTRK2 (TRKB)	2.8
ABL2 (Arg)	2.7
TNIK	2.7
NUAK1 (ARK5)	2.5
IKBKB (IKK beta)	2.2
AKT2 (PKB beta)	2.0
CLK2	1.9
AURKC (Aurora C)	1.7
BTK	1.7
CDK7/cyclin H/MNAT1	1.6
LCK	1.6
PIK3CB/PIK3R1 (p110 beta/p85 alpha)	1.6
ROS1	1.4
PRKCQ (PKC theta)	1.2
DMPK	1.2
BMX	0.9
ERBB4 (HER4)	0.9
INSRR (IRR)	0.7
FGFR4	0.5
SGK (SGK1)	0.0
LRRK2	-0.2
YES1	-0.2

IGF1R	-0.9
KDR (VEGFR2)	-1.1
PIM2	-1.5
FRAP1 (mTOR)	-1.6
EGFR (ErbB1) T790M L858R	-1.7
RPS6KB1 (p70S6K)	-2.1
JAK1	-2.3
ROCK1	-2.6
BRAF	-2.7
FLT1 (VEGFR1)	-3.1
EGFR (ErbB1)	-3.8
PAK7 (KIAA1264)	-3.8
DDR2	-4.0
PI4KB (PI4K beta)	-4.1
JAK2	-4.2
MAPK8 (JNK1)	-4.2
MAPK14 (p38 alpha) Direct	-4.4
ERBB2 (HER2)	-4.5
NEK2	-4.6
JAK3	-4.9
PAK4	-6.0
FGFR2	-6.0
KIT	-6.3
PAK2 (PAK65)	-6.9
DYRK2	-7.1
SYK	-7.5
ABL1	-8.5
PIK3CA/PIK3R1 (p110 alpha/p85 alpha)	-8.8
MINK1	-10.4
CDK2/cyclin E1	-13.7
PEAK1	-16.4
FLT3 ITD	-17.3
CAMK1 (CaMK1)	-18.7

Computational chemistry

Computational details:

All protein structures were prepared before analysis using the Protein Preparation Wizard[19] in Maestro.[20] Disordered side chains and loops missing from the structure files were modelled using Prime,[21] ligand tautomers and protonation states were assigned using Epik,[22] and protonation states of the protein and water orientations were determined and optimized at pH 7.0. Hydrogen atoms of ligand, protein, and water molecules were minimized.

Chain A of the D1228V c-MET structure bound by compound **2** was selected for computational analyses, and in which case the disordered side chain of K1110 was modelled in.

SiteMap[23, 24] calculations were performed by defining binding sites as the amino acids within 6 Å of the ligand of interest. The options of a more restrictive definition of hydrophobicity and calculation of a fine grid were used.

WaterMap[25, 26] calculations involved analyzing simulated explicit-solvent waters in the binding sites near bound ligands. Water sites within 8 Å of the ligand of interest were analyzed. X-ray waters were included and treated as solvent. Simulation time was 2.0 ns.

Analytical chemistry

High resolution mass spectrometry (HRMS)

Table S5. Gradient Elution Program of the analytical UPLC method

Time (min)	Flow Rate (mL/min)	Mobile Phase A (%)	Mobile Phase B (%)	Gradient Curve
0.00	0.4	90	10	Linear
1.50	0.4	5	95	Linear
2.00	0.4	5	95	Linear
2.30	0.4	90	10	Linear
3.00	0.4	90	10	Linear

Synthetic chemistry

Reaction schemes for multistep syntheses of compounds

Multistep synthesis of 16

Reaction scheme summary:

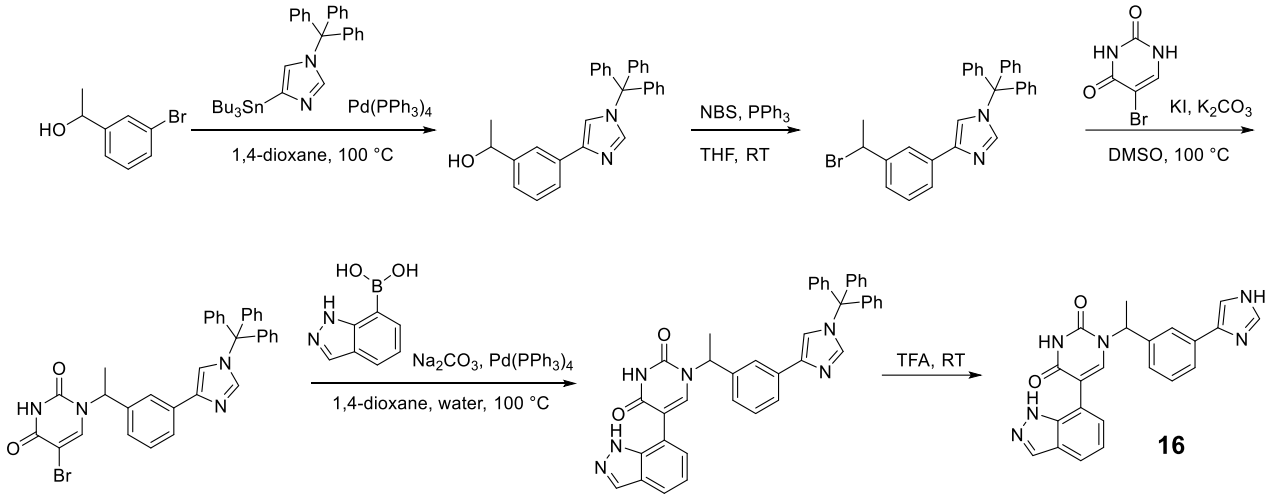

Multistep synthesis of 17

Reaction scheme summary:

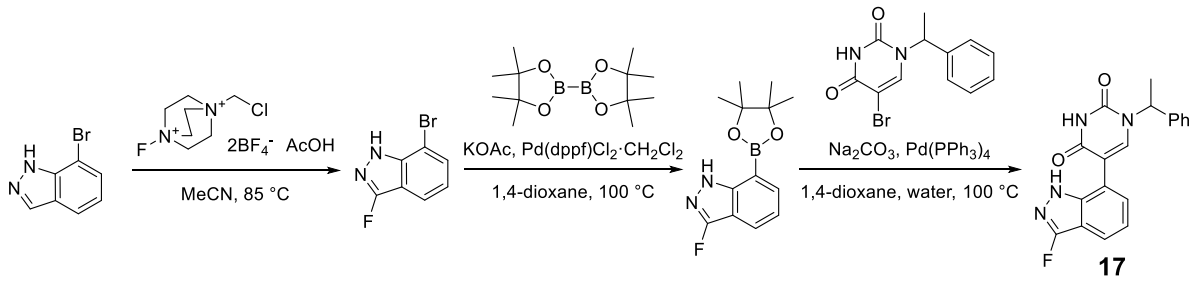

Multistep synthesis of 19

Reaction scheme summary:

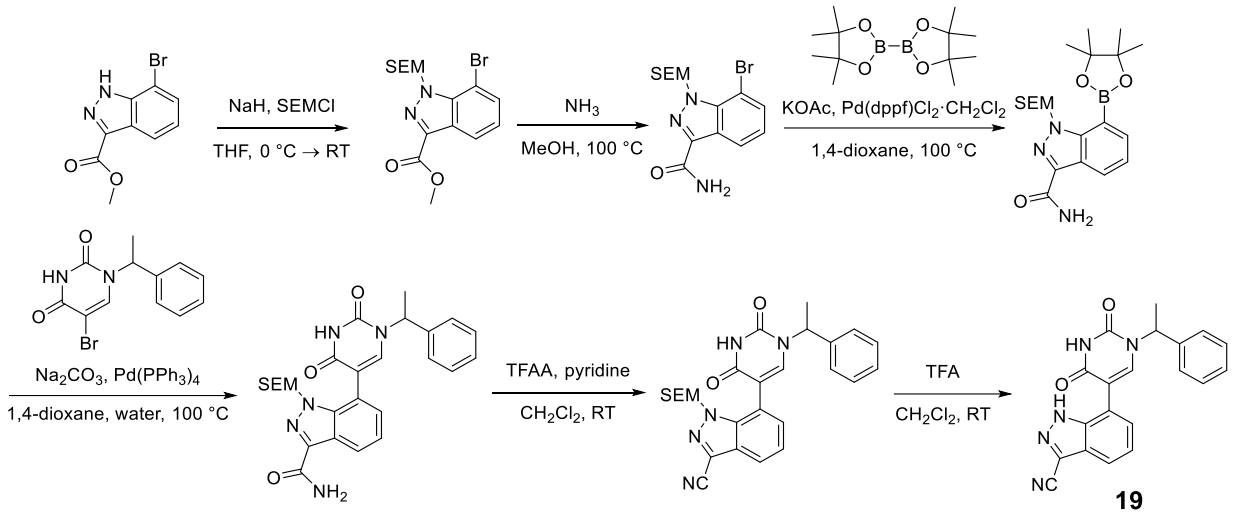

Multistep synthesis of 22

Reaction scheme summary:

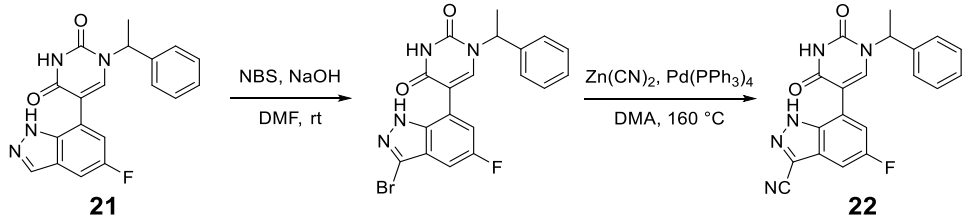

Multistep synthesis of 23

Reaction scheme summary:

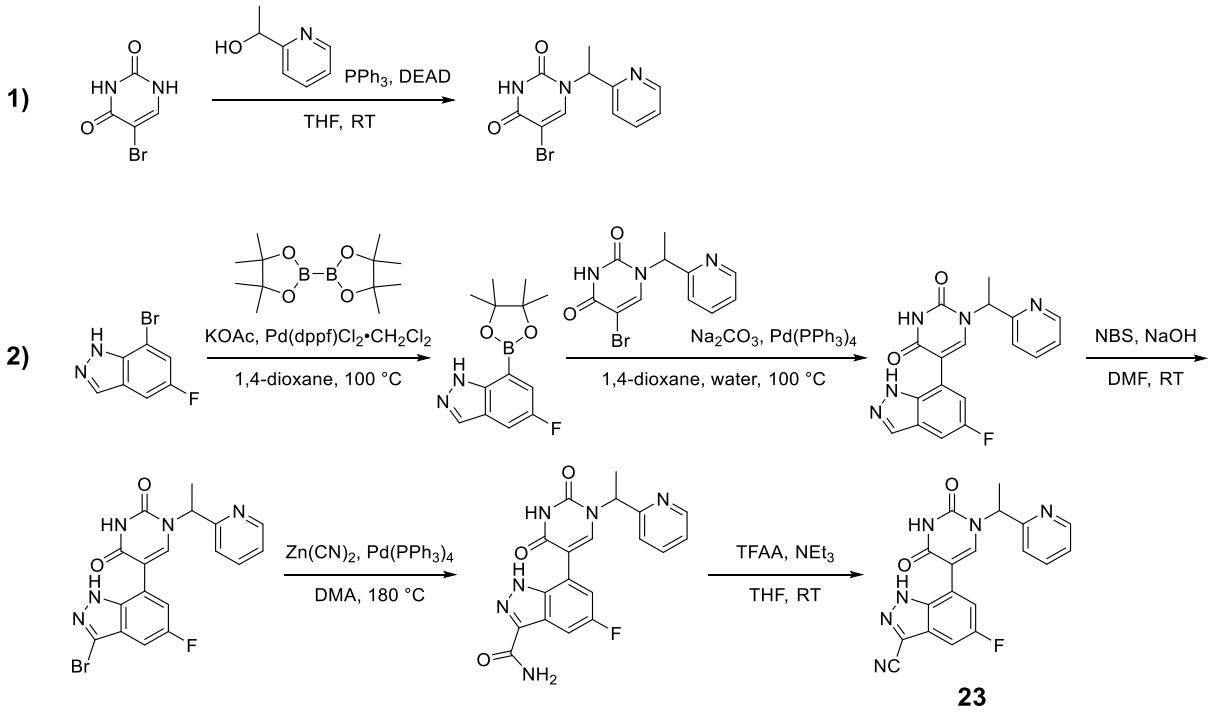

Multistep synthesis of 26, 27, 24, 25

Reaction scheme summary:

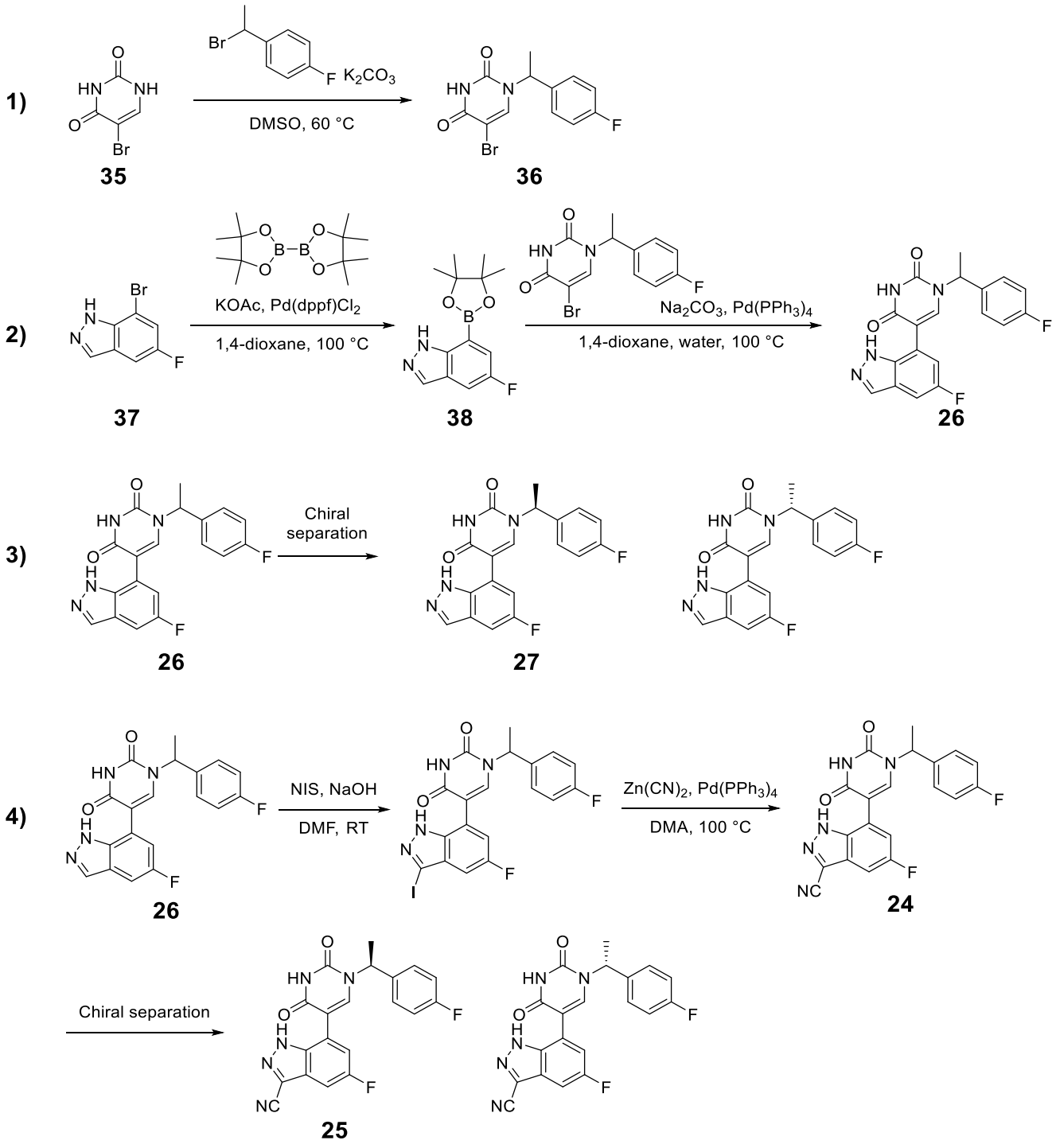

Multistep synthesis of 28

Reaction scheme summary:

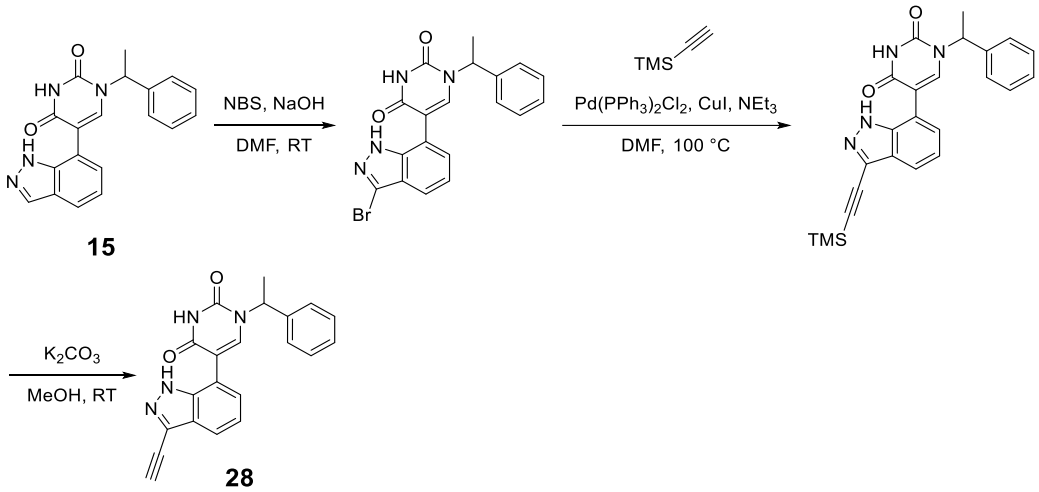

Multistep synthesis of 29 & 30

Reaction scheme summary:

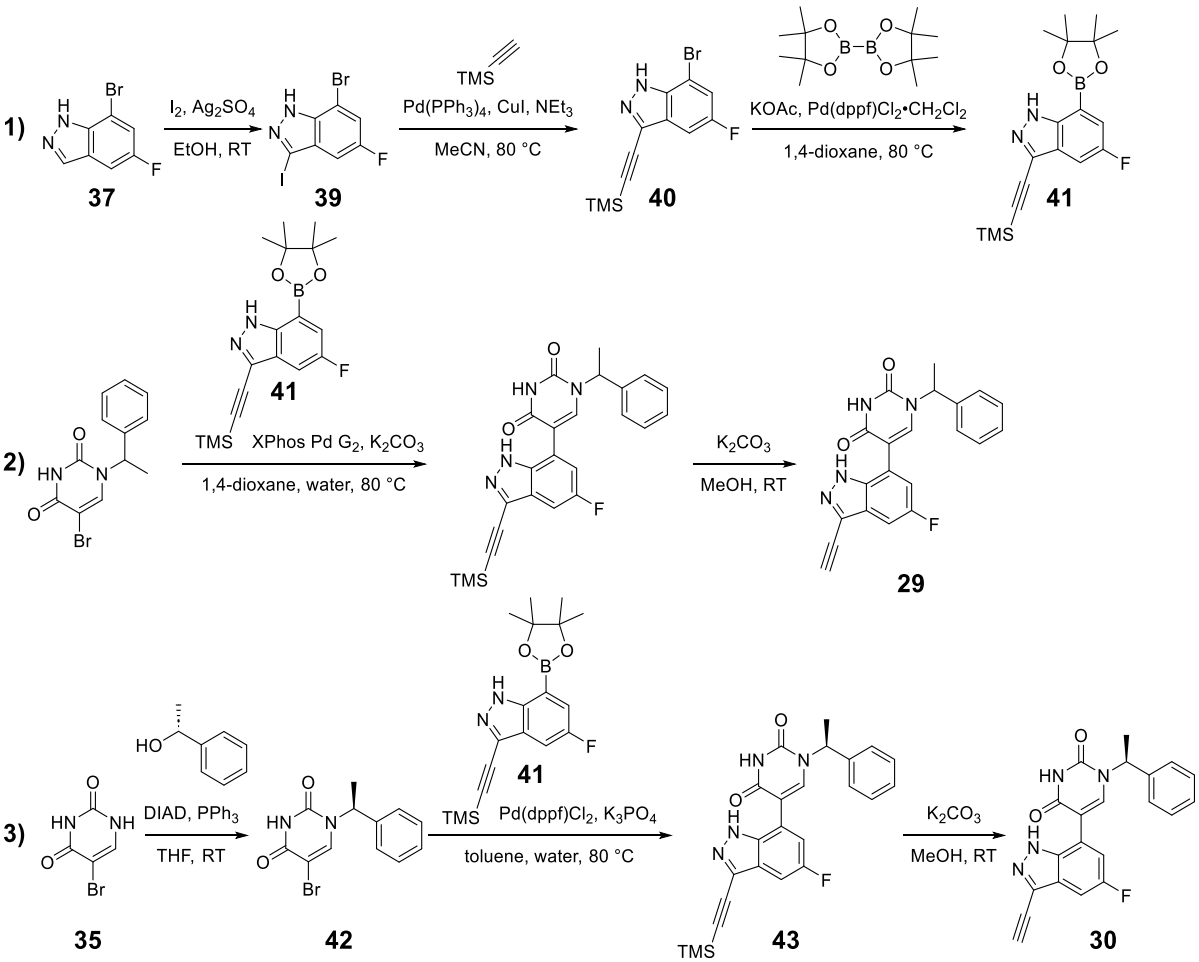

Multistep synthesis of 31 & 32

Reaction scheme summary:

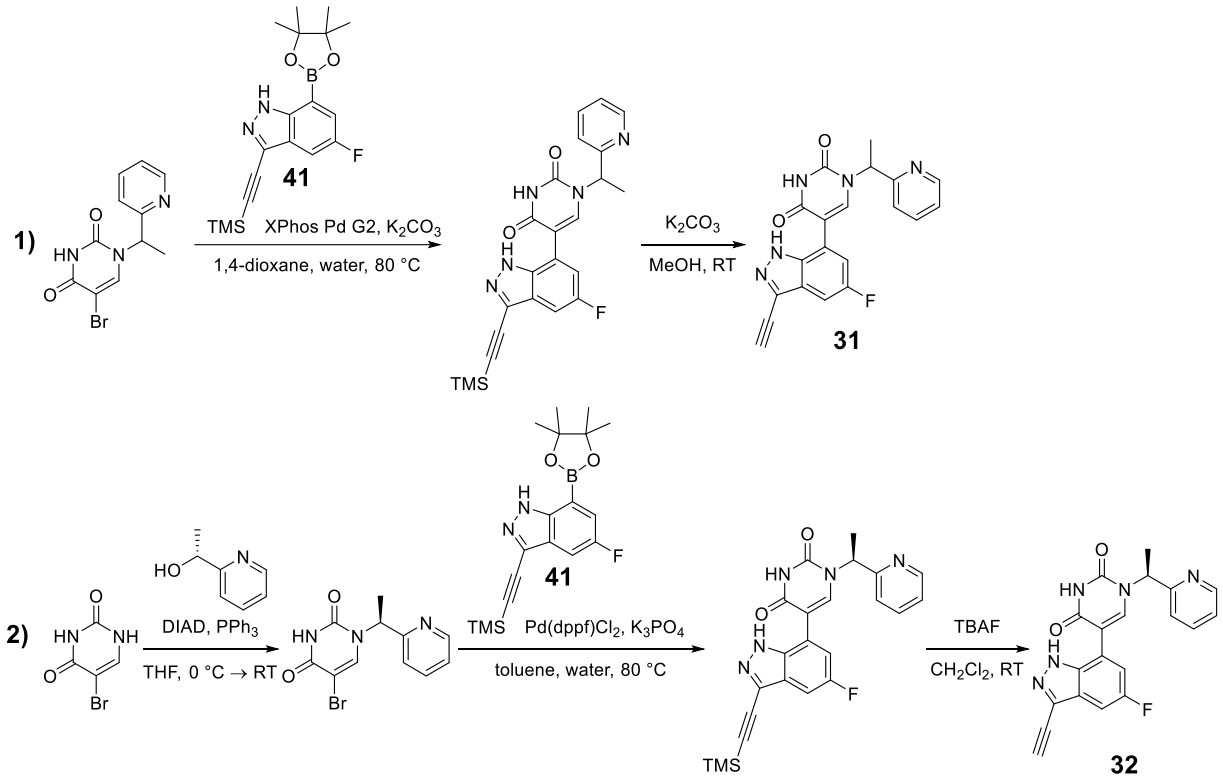

HPLC traces for *in vivo* tested compounds and key compounds:

HPLC trace of 25:

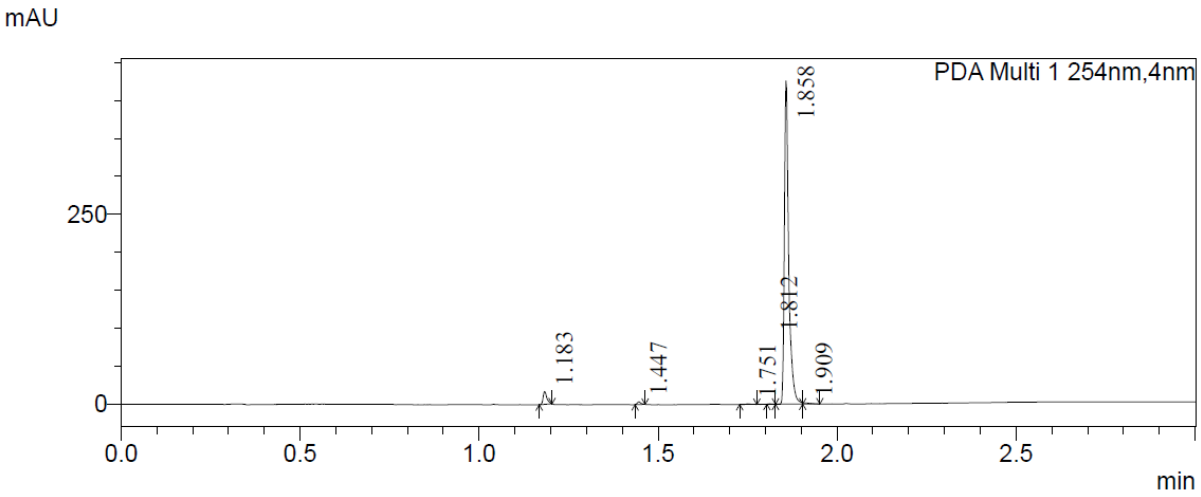

Peak Table

PDA Ch1 254nm

Peak#	Ret. Time	Height	Height%	Area	Area%
1	1.183	16351	3.799	12273	3.259
2	1.447	3475	0.807	2442	0.648
3	1.751	738	0.171	590	0.157
4	1.812	533	0.124	341	0.091
5	1.858	407664	94.723	358960	95.308
6	1.909	1616	0.376	2024	0.537
Total		430376	100.000	376630	100.000

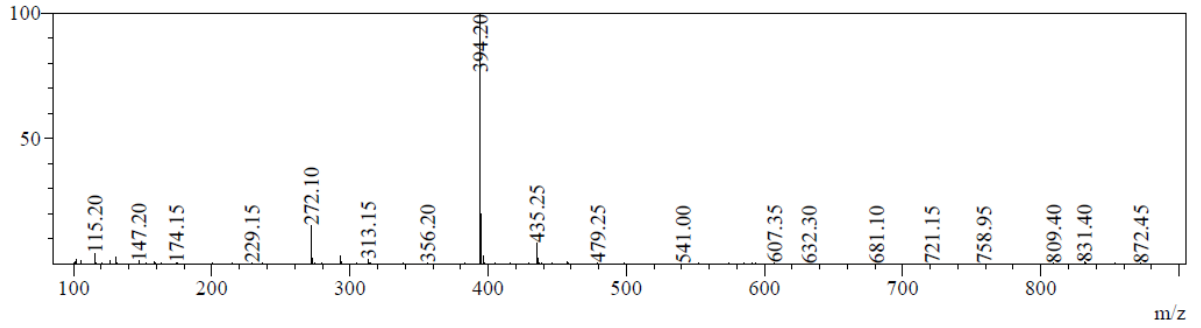

HPLC trace of 27:

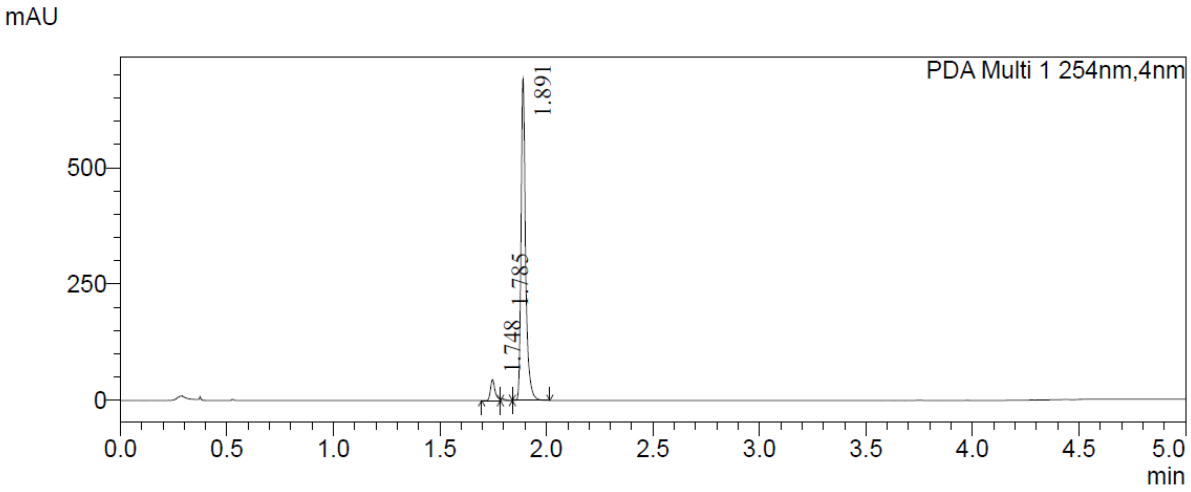

Peak Table

PDA Ch1 254nm

Peak#	Ret. Time	Height	Height%	Area	Area%
1	1.748	42968	6.161	67945	6.119
2	1.785	4311	0.618	5904	0.532
3	1.891	650082	93.220	1036551	93.349
Total		697361	100.000	1110400	100.000

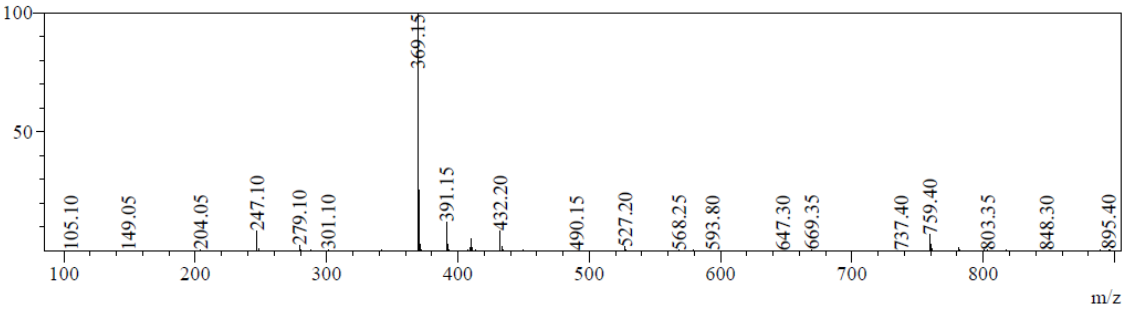

HPLC trace of 29:

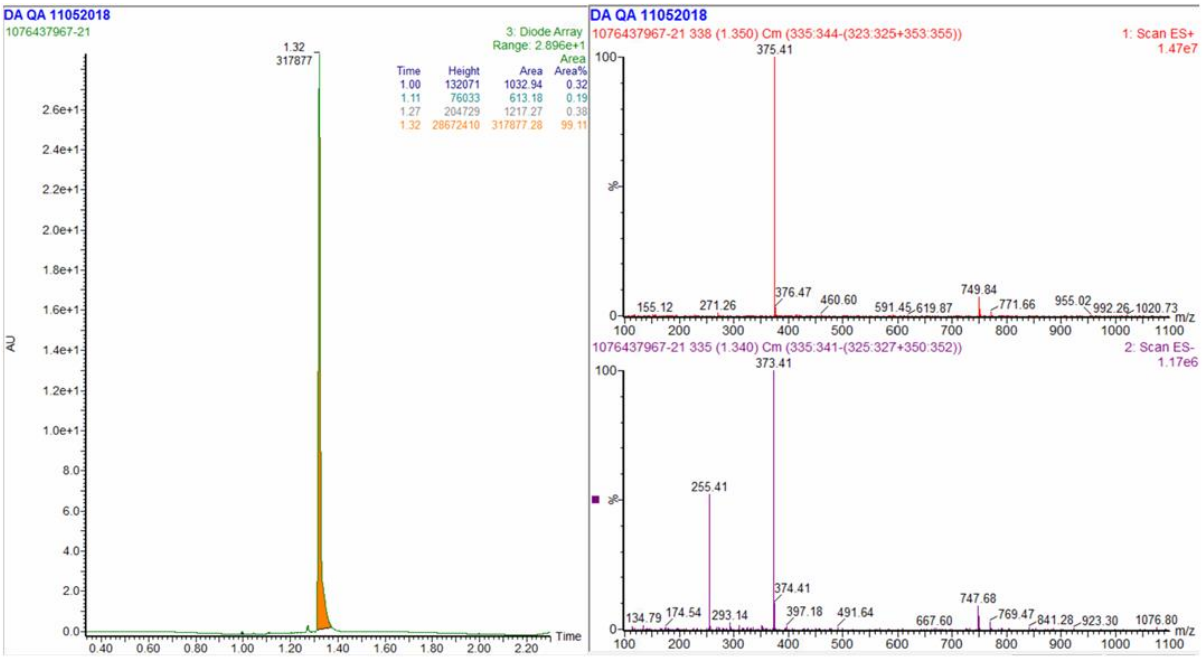

HPLC trace of 30:

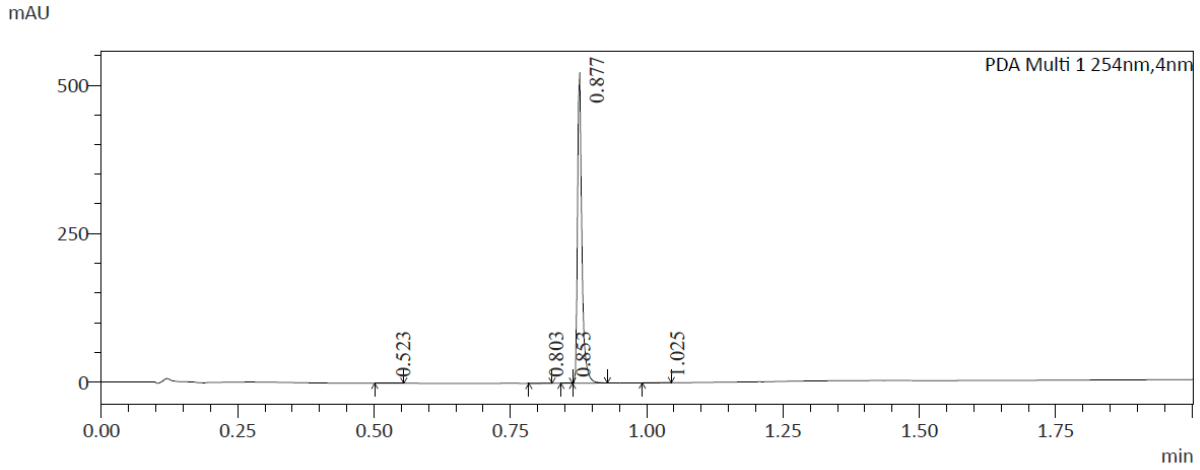

Peak Table

PDA Ch1 254nm

Peak#	Ret. Time	Height	Height%	Area	Area%
1	0.523	434	0.102	551	0.186
2	0.803	683	0.160	548	0.185
3	0.853	258	0.060	185	0.062
4	0.877	425055	99.563	293978	99.340
5	1.025	490	0.115	668	0.226
Total		426920	100.000	295930	100.000

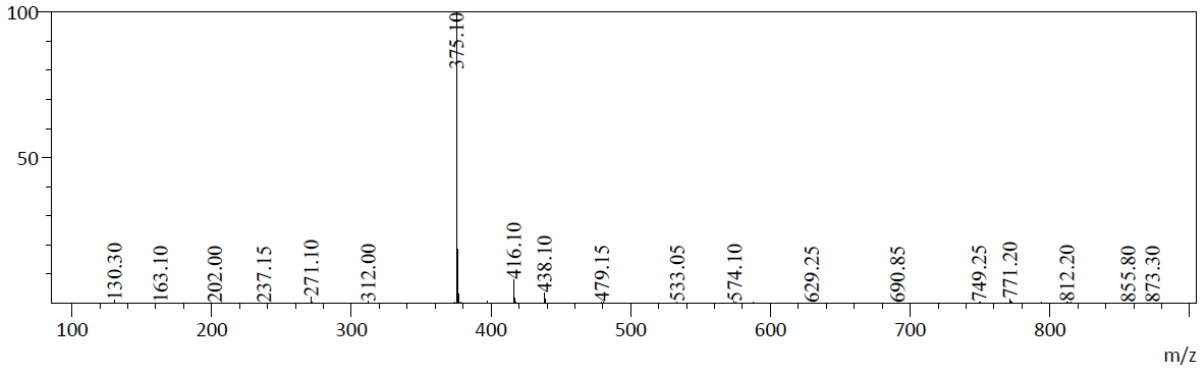

HPLC trace of 31:

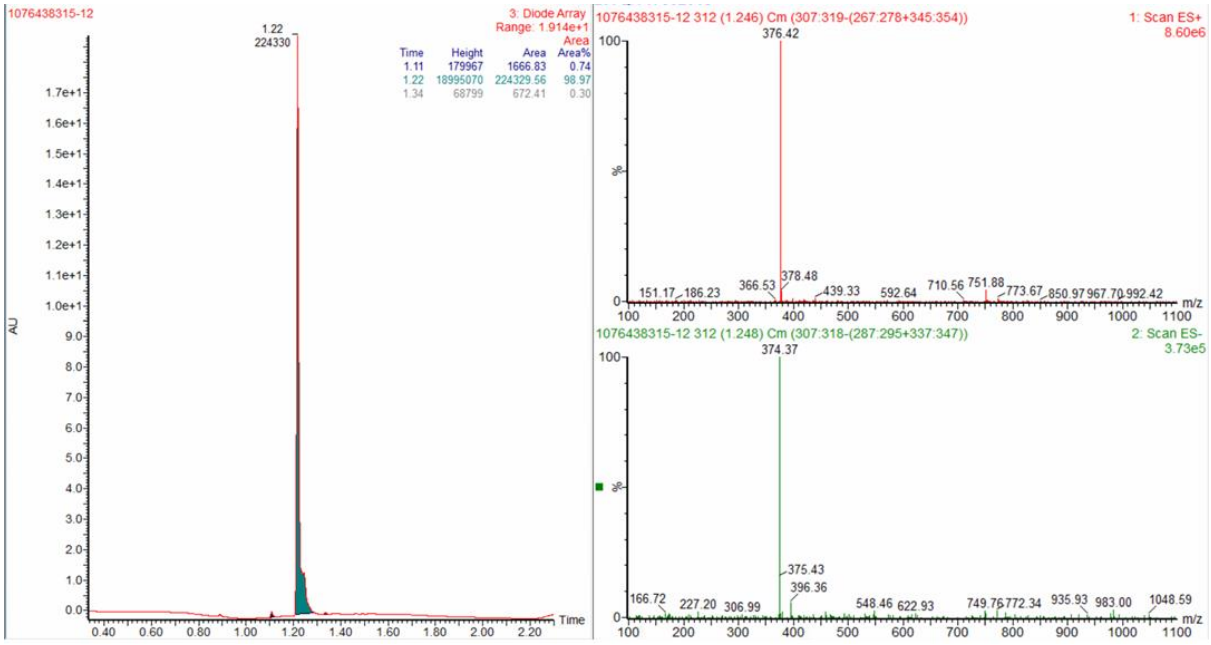

HPLC trace of 32:

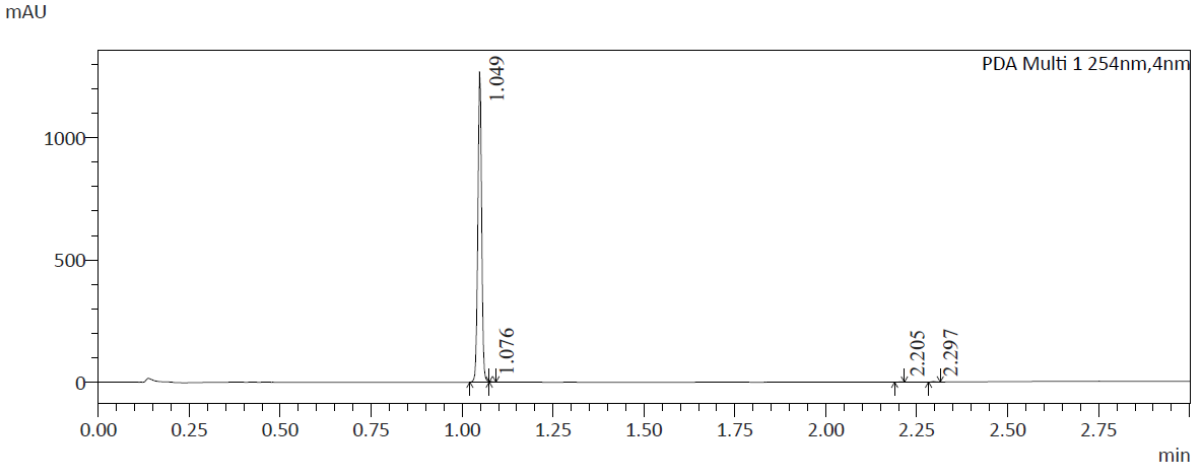

Peak Table

PDA Ch1 254nm

Peak#	Ret. Time	Height	Height%	Area	Area%
1	1.049	1271280	99.511	915305	99.677
2	1.076	3441	0.269	1238	0.135
3	2.205	892	0.070	557	0.061
4	2.297	1915	0.150	1172	0.128
Total		1277528	100.000	918271	100.000

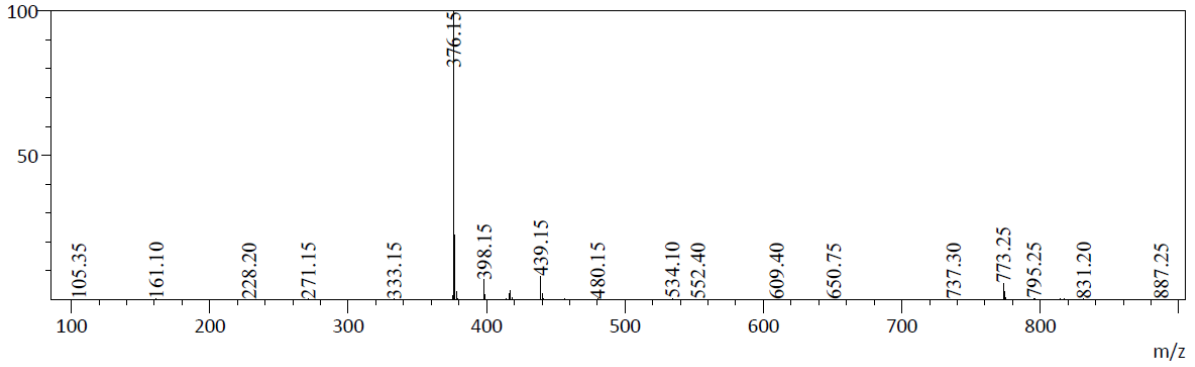

NMR spectra for key compounds

NMR spectra of 25:

^{1}H NMR (300 MHz, Methanol-d_4)

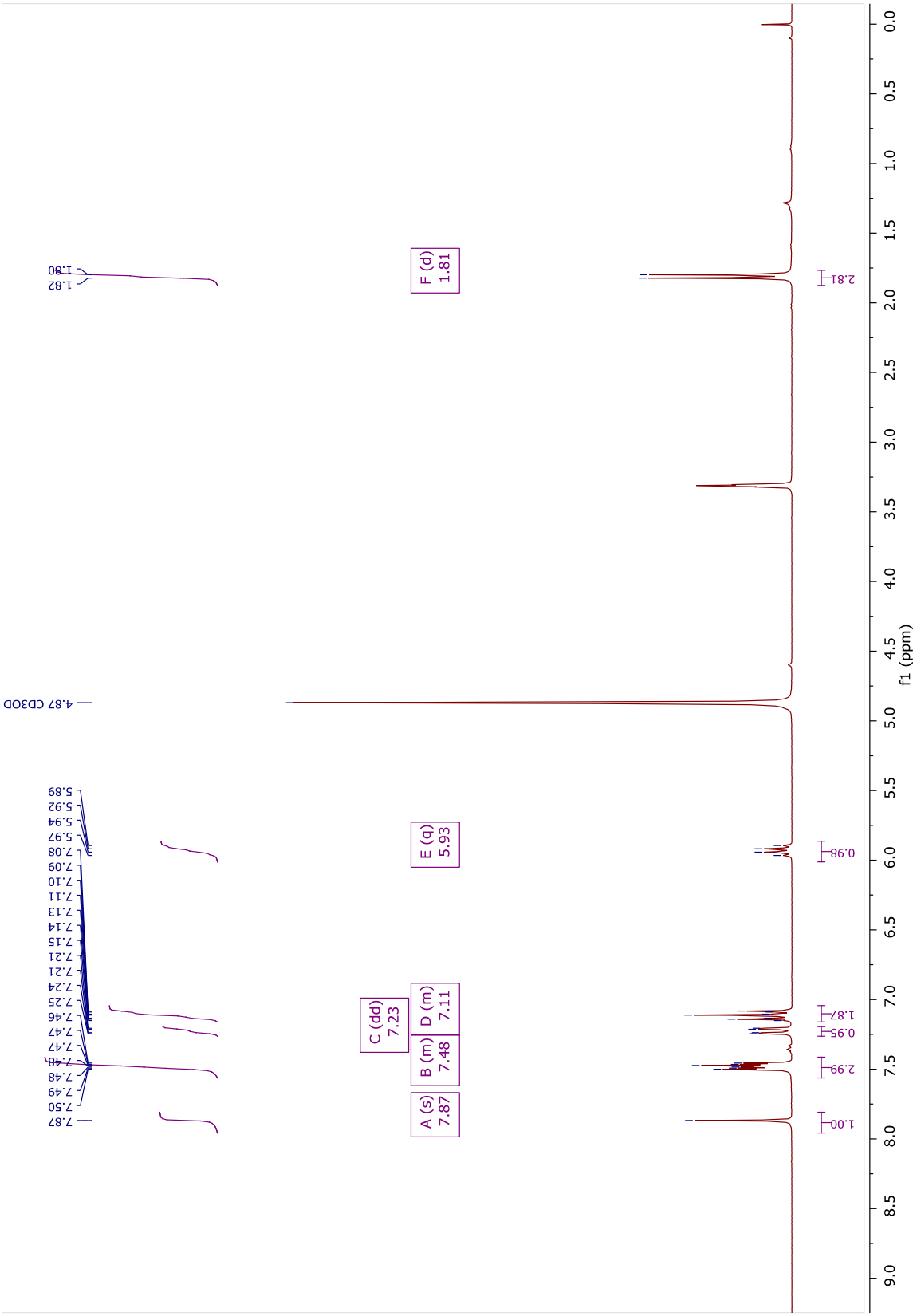

^{13}C NMR (75 MHz, Methanol-d_4)

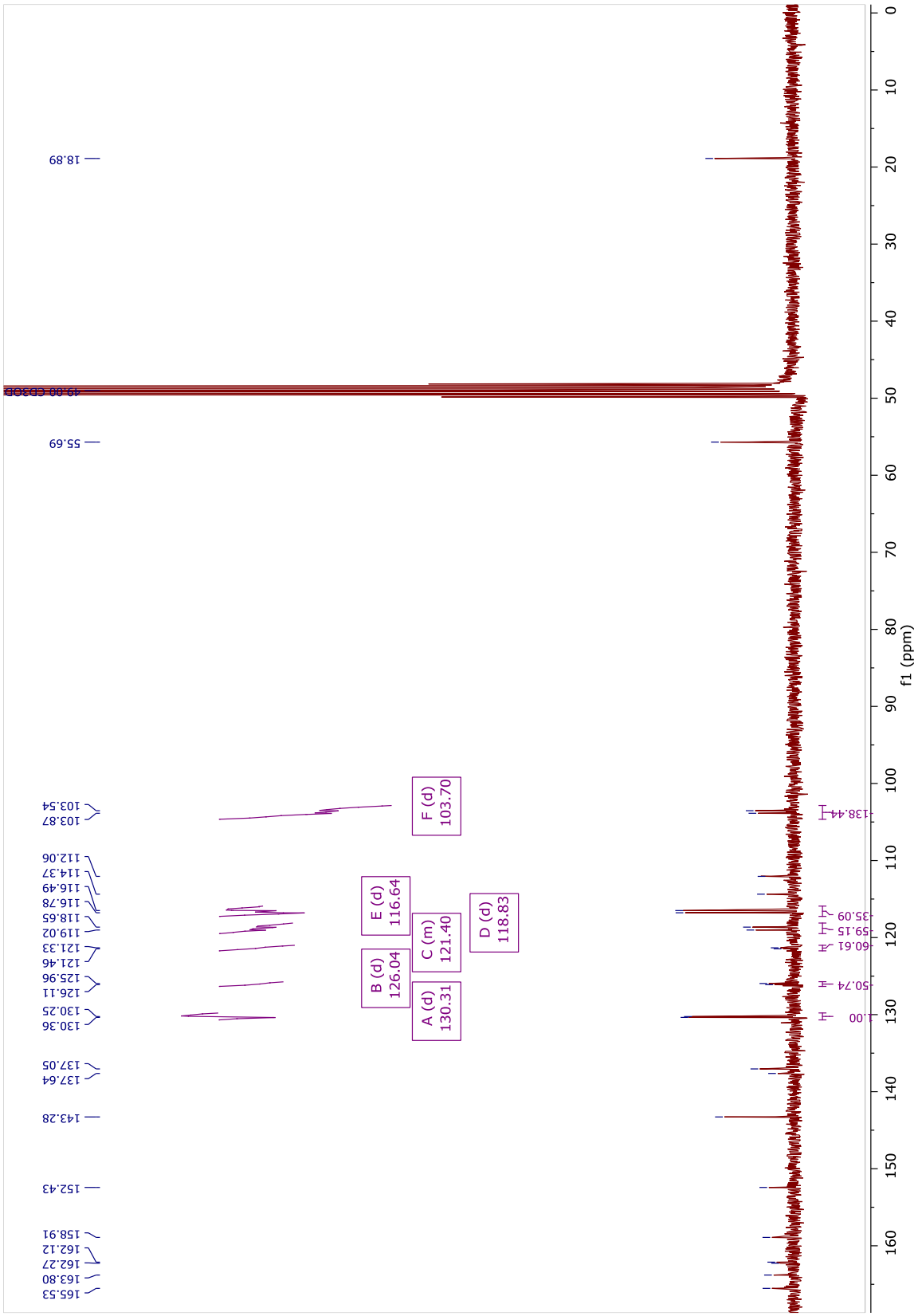

NMR spectra of 30:

^{1}H NMR (400 MHz, DMSO-d_6)

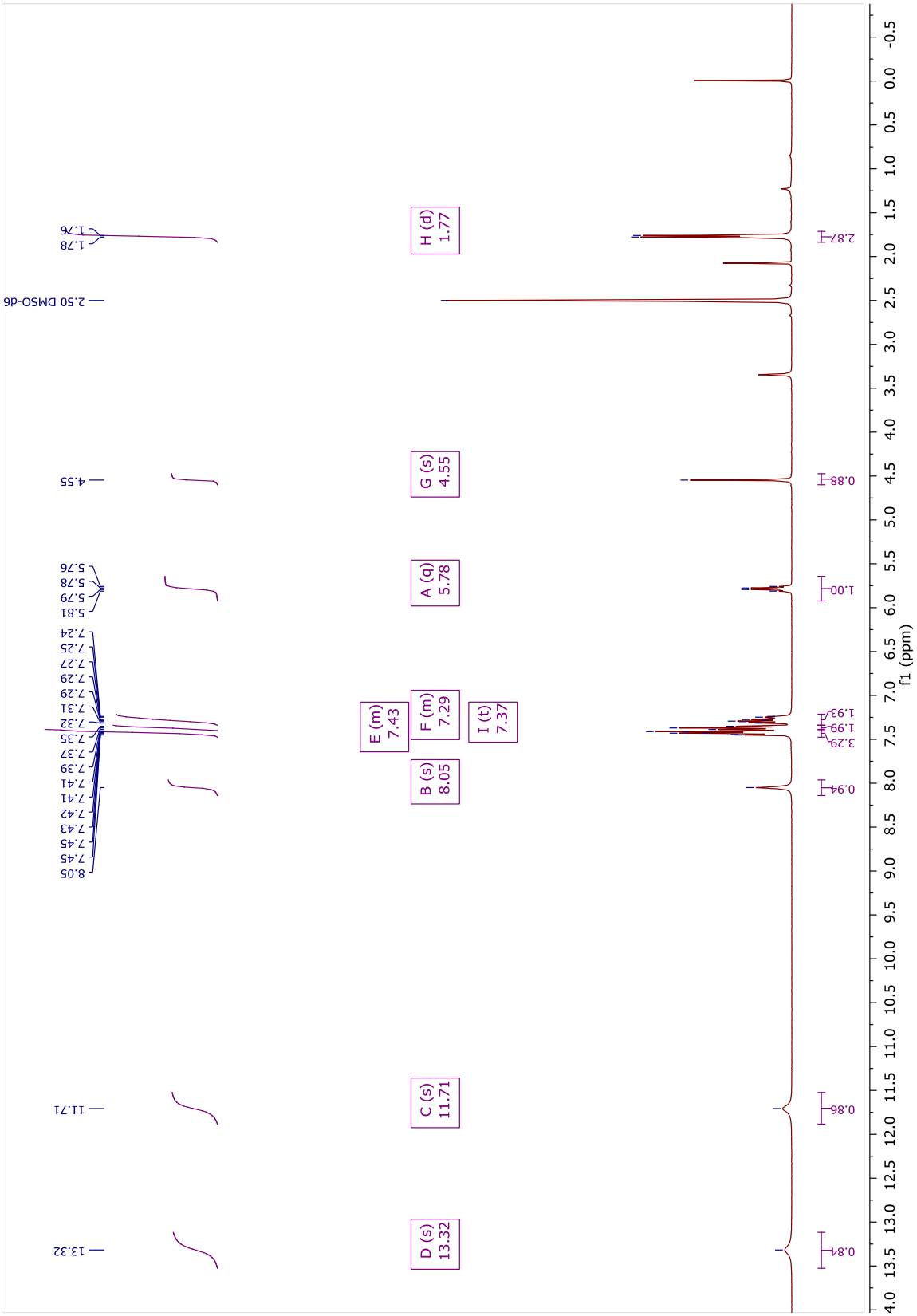

^{13}C NMR (100 MHz, DMSO-d_6)

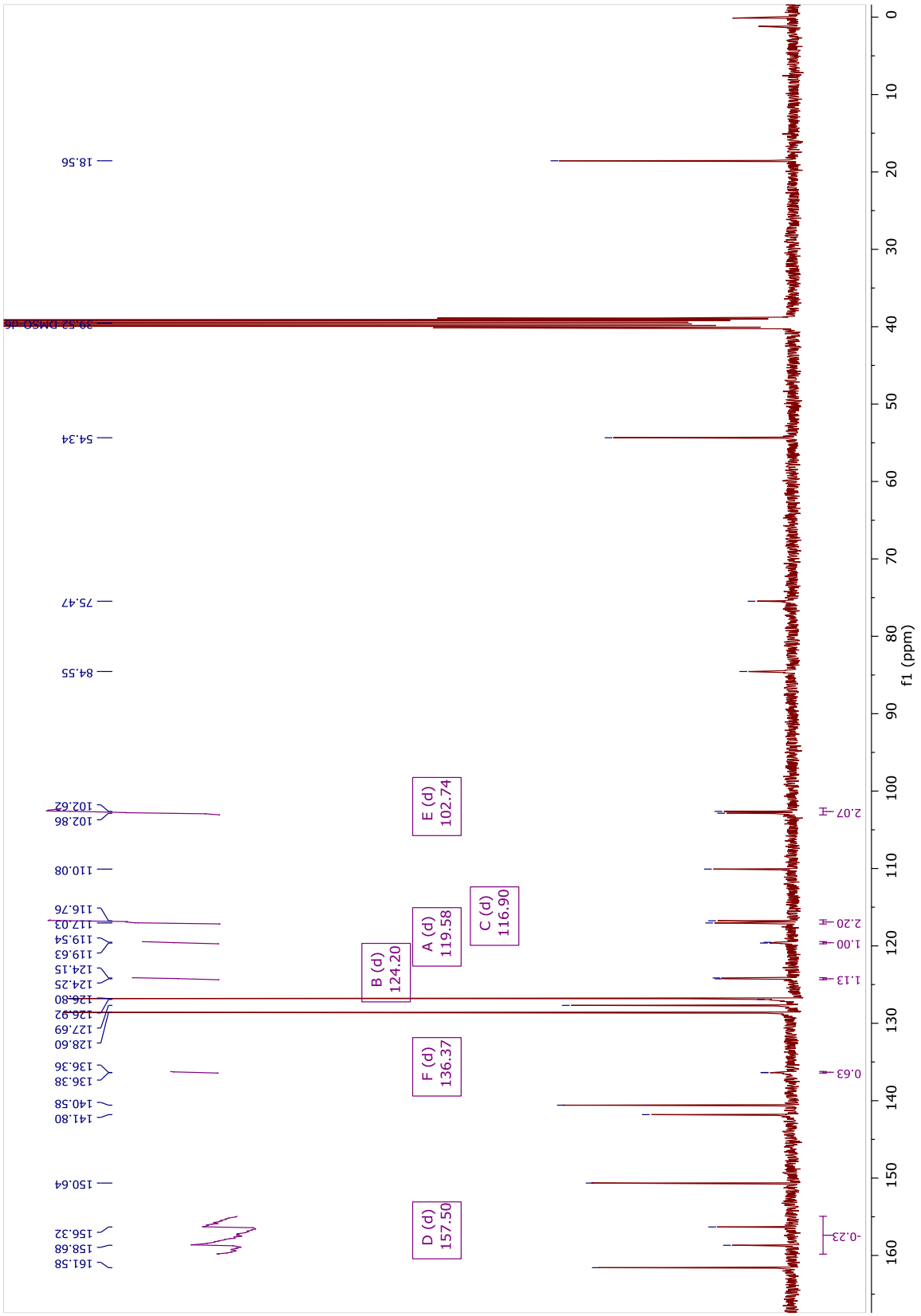

NMR spectra of 32:

^{1}H NMR (400 MHz, DMSO-d_6)

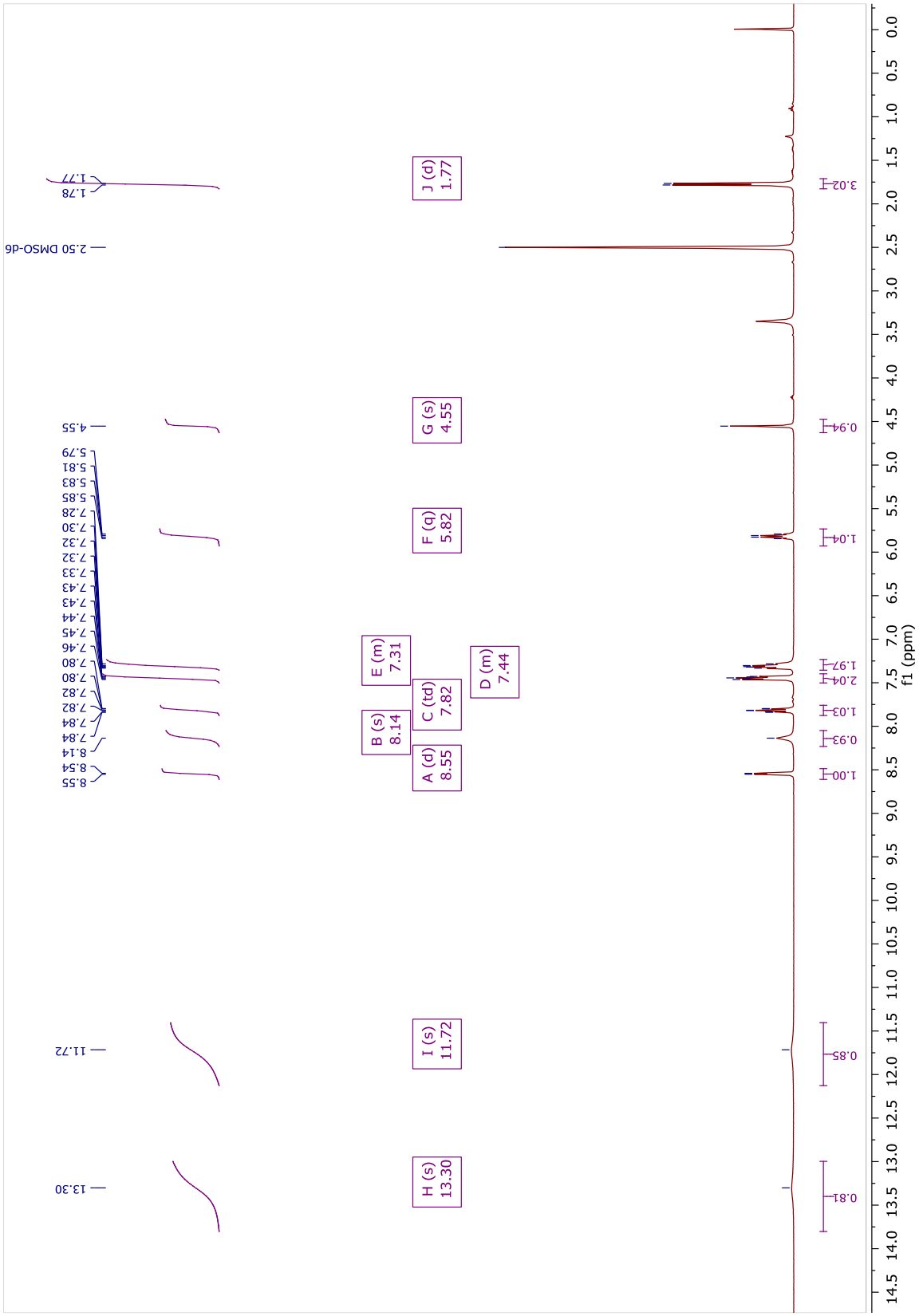

^{13}C NMR (100 MHz, DMSO-d_6)

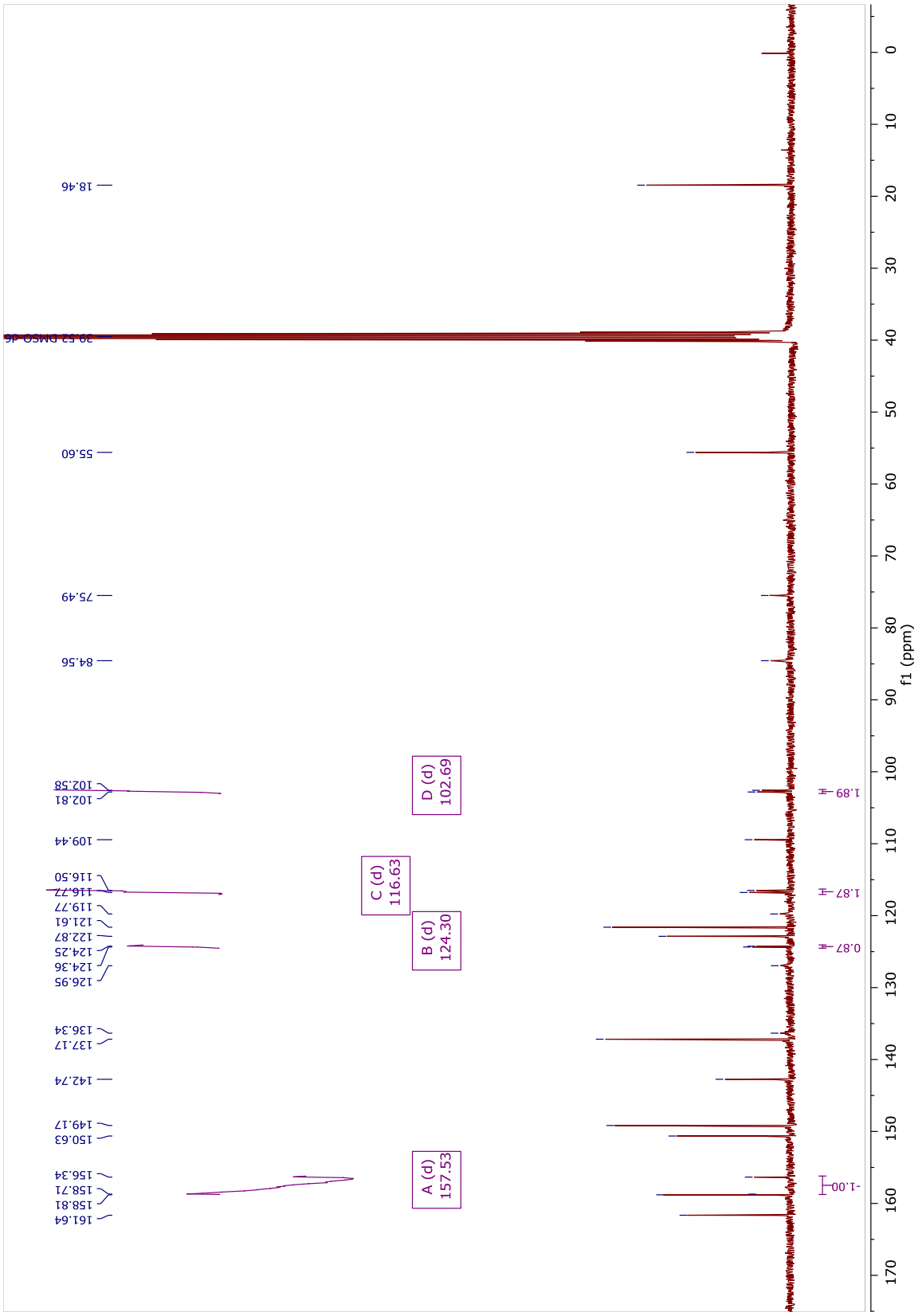

References

1. Collie, G. W.; Michaelides, I. N.; Embrey, K.; Stubbs, C. J.; Börjesson, U.; Dale, I. L.; Snijder, A.; Barlind, L.; Song, K.; Khurana, P.; Phillips, C.; Storer, R. I. Structural Basis for Targeting the Folded P-Loop Conformation of c-MET. *ACS Med. Chem. Lett.* **2021**, *12* (1), 162-167.
2. Dalvit, C.; Pevarello, P.; Tatò, M.; Veronesi, M.; Vulpetti, A.; Sundström, M. Identification of compounds with binding affinity to proteins via magnetization transfer from bulk water. *J. Biomol. NMR* **2000**, *18* (1), 65-68.
3. Collie, G. W.; Barlind, L.; Bazzaz, S.; Börjesson, U.; Dale, I. L.; Disch, J. S.; Habeshian, S.; Jetson, R.; Khurana, P.; Madin, A.; Michaelides, I. N.; Peng, L.; Snijder, A.; Stubbs, C. J. Discovery of a selective c-MET inhibitor with a novel binding mode. *Bioorg. Med. Chem. Lett.* **2022**, *75*, 128948.
4. Collie, G. W.; Koh, C. M.; O'Neill, D. J.; Stubbs, C. J.; Khurana, P.; Eddershaw, A.; Snijder, A.; Mauritzson, F.; Barlind, L.; Dale, I. L.; Shaw, J.; Phillips, C.; Hennessy, E. J.; Cheung, T.; Narvaez, A. J. Structural and Molecular Insight into Resistance Mechanisms of First Generation cMET Inhibitors. *ACS Med. Chem. Lett.* **2019**, *10* (9), 1322-1327.
5. Kabsch, W. XDS. *Acta Crystallogr. D* **2010**, *66* (Pt 2), 125-132.
6. Vonrhein, C.; Flensburg, C.; Keller, P.; Sharff, A.; Smart, O.; Paciorek, W.; Womack, T.; Bricogne, G. Data processing and analysis with the autoPROC toolbox. *Acta Crystallogr. D* **2011**, *67* (Pt 4), 293-302.
7. Winn, M. D.; Ballard, C. C.; Cowtan, K. D.; Dodson, E. J.; Emsley, P.; Evans, P. R.; Keegan, R. M.; Krissinel, E. B.; Leslie, A. G. W.; McCoy, A.; McNicholas, S. J.; Murshudov, G. N.; Pannu, N. S.; Potterton, E. A.; Powell, H. R.; Read, R. J.; Vagin, A.; Wilson, K. S. Overview of the CCP4 suite and current developments. *Acta Crystallogr. D* **2011**, *67* (Pt 4), 235-242.
8. Winter, G. xia2: an expert system for macromolecular crystallography data reduction. *J. Appl. Crystallogr.* **2010**, *43* (1), 186-190.
9. Winter, G.; Waterman, D. G.; Parkhurst, J. M.; Brewster, A. S.; Gildea, R. J.; Gerstel, M.; Fuentes-Montero, L.; Vollmar, M.; Michels-Clark, T.; Young, I. D.; Sauter, N. K.; Evans, G. DIALS: implementation and evaluation of a new integration package. *Acta Crystallogr. D* **2018**, *74* (Pt 2), 85-97.
10. McCoy, A. J.; Grosse-Kunstleve, R. W.; Adams, P. D.; Winn, M. D.; Storoni, L. C.; Read, R. J. Phaser crystallographic software. *J. Appl. Crystallogr.* **2007**, *40* (Pt 4), 658-674.
11. Collie, G. W.; Michaelides, I. N.; Embrey, K.; Stubbs, C. J.; Börjesson, U.; Dale, I. L.; Snijder, A.; Barlind, L.; Song, K.; Khurana, P.; Phillips, C.; Storer, R. I. Structural Basis for Targeting the Folded P-Loop Conformation of c-MET. *ACS Med Chem Lett* **2021**, *12* (1), 162-167.
12. Cui, J. J.; Tran-Dube, M.; Shen, H.; Nambu, M.; Kung, P. P.; Pairish, M.; Jia, L.; Meng, J.; Funk, L.; Botrous, I.; McTigue, M.; Grodsky, N.; Ryan, K.; Padrique, E.; Alton, G.; Timofeevski, S.; Yamazaki, S.; Li, Q.; Zou, H.; Christensen, J.; Mroczkowski, B.; Bender, S.; Kania, R. S.; Edwards, M. P. Structure based drug design of crizotinib (PF-02341066), a potent and selective dual inhibitor of mesenchymal-epithelial transition factor (c-MET) kinase and anaplastic lymphoma kinase (ALK). *J. Med. Chem.* **2011**, *54* (18), 6342-6363.
13. Qian, F.; Engst, S.; Yamaguchi, K.; Yu, P.; Won, K. A.; Mock, L.; Lou, T.; Tan, J.; Li, C.; Tam, D.; Lougheed, J.; Yakes, F. M.; Bentzien, F.; Xu, W.; Zaks, T.; Wooster, R.; Greshock, J.; Joly, A. H. Inhibition of tumor cell growth, invasion, and metastasis by EXEL-2880 (XL880, GSK1363089), a novel inhibitor of HGF and VEGF receptor tyrosine kinases. *Cancer Res.* **2009**, *69* (20), 8009-8016.
14. Emsley, P.; Cowtan, K. Coot: model-building tools for molecular graphics. *Acta Crystallogr. D* **2004**, *60* (Pt 12 Pt 1), 2126-2132.
15. Pflug, A.; Schimpl, M.; Nissink, J. W. M.; Overman, R. C.; Rawlins, P. B.; Truman, C.; Underwood, E.; Warwicker, J.; Winter-Holt, J.; McCoull, W. A-loop interactions in Mer tyrosine kinase give rise to inhibitors with two-step mechanism and long residence time of binding. *Biochem. J.* **2020**, *477* (22), 4443-4452.
16. Williamson, B.; Harlfinger, S.; McGinnity, D. F. Evaluation of the Disconnect between Hepatocyte and Microsome Intrinsic Clearance and In Vitro In Vivo Extrapolation Performance. *Drug Metab. Dispos.* **2020**, *48* (11), 1137-1146.

17. Fridén, M.; Ducrozet, F.; Middleton, B.; Antonsson, M.; Bredberg, U.; Hammarlund-Udenaes, M. Development of a high-throughput brain slice method for studying drug distribution in the central nervous system. *Drug Metab. Dispos.* **2009**, *37* (6), 1226-1233.
18. Fridén, M.; Winiwarter, S.; Jerndal, G.; Bengtsson, O.; Wan, H.; Bredberg, U.; Hammarlund-Udenaes, M.; Antonsson, M. Structure−Brain Exposure Relationships in Rat and Human Using a Novel Data Set of Unbound Drug Concentrations in Brain Interstitial and Cerebrospinal Fluids. *J. Med. Chem.* **2009**, *52* (20), 6233-6243.
19. Madhavi Sastry, G.; Adzhigirey, M.; Day, T.; Annabhimoju, R.; Sherman, W. Protein and ligand preparation: parameters, protocols, and influence on virtual screening enrichments. *J. Comput. Aided Mol. Des.* **2013**, *27* (3), 221-234.
20. **Schrödinger Release 2020-2:** Maestro, Schrödinger, LLC, New York, N, 2020.
21. Jacobson, M. P.; Friesner, R. A.; Xiang, Z.; Honig, B. On the Role of the Crystal Environment in Determining Protein Side-chain Conformations. *J. Mol. Biol.* **2002**, *320* (3), 597-608.
22. Greenwood, J. R.; Calkins, D.; Sullivan, A. P.; Shelley, J. C. Towards the comprehensive, rapid, and accurate prediction of the favorable tautomeric states of drug-like molecules in aqueous solution. *J. Comput. Aided Mol. Des.* **2010**, *24* (6), 591-604.
23. Halgren, T. New Method for Fast and Accurate Binding-site Identification and Analysis. *Chem. Biol. Drug Des.* **2007**, *69* (2), 146-148.
24. Halgren, T. A. Identifying and Characterizing Binding Sites and Assessing Druggability. *J. Chem. Inf. Model.* **2009**, *49* (2), 377-389.
25. Abel, R.; Young, T.; Farid, R.; Berne, B. J.; Friesner, R. A. Role of the active-site solvent in the thermodynamics of factor Xa ligand binding. *J. Am. Chem. Soc.* **2008**, *130* (9), 2817-2831.
26. Young, T.; Abel, R.; Kim, B.; Berne, B. J.; Friesner, R. A. Motifs for molecular recognition exploiting hydrophobic enclosure in protein–ligand binding. *Proc. Natl. Acad. Sci. U.S.A.* **2007**, *104* (3), 808-813.